

Semiparametric Efficient Test for Interpretable Distributional Treatment Effects

Houssam Zenati¹ and Arthur Gretton¹

¹Gatsby Computational Neuroscience Unit, University College London

Abstract

Distributional treatment effects can be invisible to means: a treatment may preserve average outcomes while changing tails, modes, dispersion, or rare-event probabilities. Kernel tests can detect discrepancies between interventional outcome laws, but global tests do not reveal where the laws differ. We propose DR-ME, to our knowledge the first semiparametrically efficient finite-location test for interpretable distributional treatment effects. DR-ME evaluates an interventional kernel witness at learned outcome locations, returning causal-discrepancy coordinates rather than only a global rejection. From observational data, we derive orthogonal doubly robust kernel features whose centered oracle form is the canonical gradient of this finite witness. For fixed locations, we characterize the local testing limit: DR-ME is chi-square calibrated under the null, has noncentral chi-square local power, and uses the covariance whitening that optimizes local signal-to-noise for discrepancies visible through the selected coordinates. This efficient local-power geometry yields a principled location-learning criterion, with sample splitting preserving post-selection validity. Experiments show near-nominal type-I error, competitive power against global doubly robust kernel tests, and interpretable learned locations that localize distributional effects in a semi-synthetic medical-imaging study.

1 Introduction

Average treatment effects are often too coarse for causal questions involving risk, heterogeneity, or structured outcomes. A treatment may leave the mean outcome nearly unchanged while altering dispersion, tails, multimodality, or the probability of rare but consequential events. This is the motivation behind distributional treatment-effect analysis, including nonparametric policy effects [30] and inference on interventional distributions [3]. The issue is even sharper when outcomes are images, sequences, graphs, embeddings, or high-dimensional measurements [8]: reducing such outcomes to a small number of hand-chosen scalar summaries can obscure the effect of interest. We therefore study tests of interventional outcome distributions, rather than tests that only address average effects.

Kernel mean embeddings provide a natural language for this task. They represent probability laws as elements of a reproducing kernel Hilbert space [34], so that distributional discrepancies can be studied without first specifying a scalar outcome summary. With characteristic kernels, equality of embeddings is equivalent to equality of probability laws [35]. The associated RKHS distance is the maximum mean discrepancy, a central tool in kernel two-sample testing [9]. In causal problems, counterfactual mean embeddings extend this representation to potential-outcome laws [24], and counterfactual policy mean embeddings extend it to policy-induced outcome distributions with doubly robust estimation [40].

Global kernel discrepancies are powerful omnibus tools, but they are often hard to interpret. A global rejection says that two interventional outcome laws differ, but not where the difference is expressed. Recent doubly robust kernel tests make global RKHS discrepancies available for observational causal studies [6, 23, 41], but their evidence remains fundamentally global. In ordinary two-sample testing, finite-location mean-embedding tests address this limitation by evaluating a witness function at a small number of spatial or

frequency locations [5, 16]. These locations act as interpretable distributional features: they indicate where two laws are most distinguishable after accounting for sampling variability. In observational causal problems, however, the corresponding oracle contrast involves both potential outcomes, so naive treated-versus-control finite-location features are confounded and invalid.

Our work is also related to semiparametric tests beyond scalar parameters. Restricted score tests target function-valued risk minimizers by testing risk derivatives over restricted direction classes [14]. Global MMD tests for unknown functions compare distributions of estimated functions and rely on higher-order pathwise differentiability [22]. Hilbert-valued one-step theory gives efficient inference for RKHS-valued parameters, including counterfactual mean embeddings [21]. These works address different inferential objects: restricted score tests, global MMD tests, or Hilbert-valued confidence sets. Here we target a finite-location projection of an interventional kernel witness. This finite projection gives interpretable outcome-space coordinates, admits a first-order canonical gradient, and leads to an efficient finite-dimensional local testing geometry that can be used to learn where to test.

We develop DR-ME, a semiparametrically efficient finite-location test for causal distributional testing. The locations are interpretable causal-discrepancy coordinates: each asks whether the interventional laws differ through their kernel similarity to a selected outcome point. The challenge is that these coordinates are features of interventional laws, not of observed treated and control samples. Under selection on observables and positivity [11, 15, 29, 31], they are identified through propensity scores and outcome regressions, but identification alone is not enough for nuisance-robust inference. We therefore derive an orthogonal augmented inverse-propensity feature. For fixed locations, it has the usual doubly robust structure [1, 10, 28]; with cross-fitting, its empirical mean has a first-order expansion whose leading term is the canonical gradient of the finite-location signal, while nuisance errors enter through second-order remainders [4].

One of our main contributions is a semiparametric local-efficiency theory for this finite-location causal test. For fixed locations, we study quadratic-mean-differentiable local submodels through the finite-location null, following the local asymptotic testing perspective of Neyman and Pearson [25], Le Cam and Yang [20], and van der Vaart [36]. The canonical-gradient statistic attains the efficient finite-signal Gaussian experiment. Consequently, the Hotelling statistic [13] has a chi-square null limit and a noncentral chi-square local limit, with power governed by the interventional drift whitened by the canonical-gradient covariance. This whitening is not an accidental consequence of plugging a doubly robust score into a conventional Hotelling statistic; it is the covariance geometry of the efficient finite-signal experiment.

This geometry also determines how locations should be learned. The relevant objective is not the raw witness magnitude, but its magnitude after whitening by the canonical-gradient covariance. We therefore learn locations by maximizing a ridge-stabilized empirical local-power criterion. Locations are selected on an auxiliary split and tested on an independent final split; conditional on the learning split, the selected locations are fixed, so the fixed-location null theory applies after selection [7, 19]. Experiments on synthetic and semi-synthetic structured outcomes show calibrated type-I error, competitive power relative to global doubly robust kernel tests [6, 23, 40], and learned locations that localize distributional shifts.

Our contributions are fourfold. First, we formulate interpretable finite-location testing for distributional treatment effects by evaluating the interventional RKHS witness at selected outcome locations. Second, we derive the canonical gradient of this finite signal; its augmented inverse-propensity form yields an orthogonal doubly robust feature, whose cross-fitted version defines the DR-ME Hotelling statistic. We show that DR-ME attains the efficient finite-signal Gaussian experiment, giving chi-square calibration, noncentral local power, and canonical-gradient covariance whitening. Third, we use this geometry to learn locations and prove uniform consistency of the empirical criterion. Fourth, we validate calibration, power, and covariance-whitened location learning in simulations, and use a semi-synthetic medical-imaging study to show that learned locations can localize distributional causal effects nearly invisible to mean contrasts.

Section 2 defines the finite-location causal witness and derives the doubly robust observed-data feature whose centered oracle form is the canonical gradient. Section 3 develops the fixed-location local testing theory, including chi-square calibration, noncentral chi-square local power, and the efficient covariance geometry underlying the Hotelling statistic. Section 4 uses this geometry to construct the location-learning criterion and proves uniform consistency of its empirical version under sample splitting. Section 5 evaluates calibration,

power, covariance-whitened location learning, and image-space interpretability.

2 Finite-location causal witnesses and observed-data scores

We use the potential-outcomes notation [15, 31]. Let $A \in \{0, 1\}$ be a binary treatment, let $Y(0), Y(1) \in \mathcal{Y}$ be potential outcomes, and let k_Y be a bounded positive definite kernel on \mathcal{Y} , with RKHS \mathcal{H}_Y and feature map $\varphi_Y(y) = k_Y(\cdot, y)$. For each arm a , define the interventional mean embedding $\chi(a) := \mathbb{E}[\varphi_Y(Y(a))]$, following counterfactual and policy mean embedding constructions [24, 40]. The interventional embedding difference is $\Delta := \chi(1) - \chi(0)$, with witness function

$$w(y) := \langle \Delta, \varphi_Y(y) \rangle_{\mathcal{H}_Y} = \mathbb{E}[k_Y(y, Y(1))] - \mathbb{E}[k_Y(y, Y(0))]. \quad (1)$$

Thus $w(y)$ is the kernel discrepancy between the two interventional outcome laws near location y . Moreover, $\|\Delta\|_{\mathcal{H}_Y}^2$ is the squared maximum mean discrepancy between $P_{Y(1)}$ and $P_{Y(0)}$ [9]; if k_Y is characteristic, then $\Delta = 0$ is equivalent to equality of the two interventional outcome laws [35].

To obtain an interpretable finite signal, fix $J \geq 1$ outcome locations $V = (v_1, \dots, v_J) \in \mathcal{Y}^J$, and write $k_V(y) := (k_Y(v_1, y), \dots, k_Y(v_J, y))^\top \in \mathbb{R}^J$. The finite-location causal witness is

$$\mu_V := (w(v_1), \dots, w(v_J))^\top = \mathbb{E}[k_V(Y(1))] - \mathbb{E}[k_V(Y(0))] \in \mathbb{R}^J. \quad (2)$$

This is a finite-dimensional projection of the RKHS discrepancy Δ , with coordinates indexed by interpretable outcome locations. The global null $H_0 : \Delta = 0$ implies the finite-location null $H_{0,V} : \mu_V = 0$ for every V . Conversely, a fixed finite V need not characterize every global alternative. The procedure is therefore calibrated under the global causal null, with power against alternatives visible through the selected witness coordinates. This follows the finite-location mean-embedding testing principle of Chwialkowski et al. [5] and Jitkrittum et al. [16], but for interventional rather than ordinary two-sample distributions.

If samples from $P_{Y(1)}$ and $P_{Y(0)}$ were directly available, the problem would reduce to a J -dimensional mean test based on the oracle contrasts $k_V(Y^{(1)}) - k_V(Y^{(0)})$. In observational data, these contrasts are unavailable because each unit reveals only one potential outcome. We therefore construct an observed-data pseudo-feature whose mean is μ_V and whose centered form is the canonical gradient of this finite-location signal.

Identification. Let $Z = (X, A, Y) \sim P_0$. We assume consistency, $Y = Y(a)$ when $A = a$; conditional exchangeability, $Y(a) \perp A \mid X$; and positivity, $\pi_0(a \mid X) := P_0(A = a \mid X) \geq \varepsilon > 0$ almost surely, for $a \in \{0, 1\}$ [11, 29]. For fixed V , define

$$m_a(x; V) := \mathbb{E}[k_V(Y) \mid A = a, X = x], \quad \mu_{a,V} := \mathbb{E}[k_V(Y(a))]. \quad (3)$$

Then $\mu_{a,V} = \mathbb{E}[m_a(X; V)]$, and hence $\mu_V = \mathbb{E}[m_1(X; V) - m_0(X; V)]$. Thus μ_V is identified by a regression contrast, but the feasible plug-in contrast is not orthogonal to nuisance error: regression estimation error induces first-order bias. We therefore use an augmented score whose moment is locally insensitive to nuisance perturbations, so that first-stage errors enter only through higher-order remainders [4].

Orthogonal observed-data feature. Let $\eta = (\pi, r_0, r_1)$ be a nuisance tuple, where $\pi(a \mid x) > 0$ is a propensity model and $r_a(x; V) \in \mathbb{R}^J$ is a candidate regression for $m_a(x; V)$. Define the arm-specific augmented feature

$$\phi_V^a(Z; \eta) := \frac{\mathbf{1}\{A = a\}}{\pi(a \mid X)} (k_V(Y) - r_a(X; V)) + r_a(X; V), \quad a \in \{0, 1\},$$

and the doubly robust contrast $z_V^{\text{dr}}(Z; \eta) := \phi_V^1(Z; \eta) - \phi_V^0(Z; \eta)$. This is the vector-valued analogue of augmented inverse-propensity scores [1, 10, 28].

Proposition 2.1 (Doubly robust feature and canonical gradient). *Assume the identification conditions above. For any nuisance tuple $\eta = (\pi, r_0, r_1)$ with $\pi(a | X) > 0$ almost surely,*

$$\mathbb{E}\{\phi_V^a(Z; \eta)\} - \mu_{a,V} = \mathbb{E}\left[\frac{\pi_0(a | X) - \pi(a | X)}{\pi(a | X)}\{m_a(X; V) - r_a(X; V)\}\right].$$

Consequently, $\mathbb{E}\{\phi_V^a(Z; \eta)\} = \mu_{a,V}$ if either $\pi(a | \cdot) = \pi_0(a | \cdot)$ or $r_a(\cdot; V) = m_a(\cdot; V)$. Let $\eta_0 = (\pi_0, m_0, m_1)$. Then $\mathbb{E}\{z_V^{\text{dr}}(Z; \eta_0)\} = \mu_V$, and

$$\psi_V(Z) := z_V^{\text{dr}}(Z; \eta_0) - \mu_V$$

is the canonical gradient of μ_V in the nonparametric model.

For the full RKHS-valued counterfactual mean embedding, the corresponding Hilbert-valued pathwise differentiability and efficient influence function are established by Luedtke and Chung [21]; here we use the finite-dimensional projection induced by fixed locations. The proof is given in Appendix C. Proposition 2.1 has two roles. First, its bias identity gives the orthogonality mechanism: the target-moment error is a product of propensity and outcome-regression errors. Second, the centered augmented contrast is the canonical gradient of the finite witness, which is the link to local testing efficiency. The statistic below is built from this canonical-gradient representation.

DR-ME statistic. Let $Z_1, \dots, Z_n \stackrel{\text{i.i.d.}}{\sim} P_0$. For each i , let $\hat{\eta}_{-i}$ be a nuisance estimate trained on data independent of Z_i ; this notation covers both K -fold cross-fitting and the independent nuisance split used after location learning. Define

$$\hat{z}_{i,V}^{\text{dr}} := z_V^{\text{dr}}(Z_i; \hat{\eta}_{-i}), \quad \bar{z}_{n,V}^{\text{dr}} := \frac{1}{n} \sum_{i=1}^n \hat{z}_{i,V}^{\text{dr}}, \quad S_{n,V}^{\text{dr}} := \frac{1}{n-1} \sum_{i=1}^n (\hat{z}_{i,V}^{\text{dr}} - \bar{z}_{n,V}^{\text{dr}})(\hat{z}_{i,V}^{\text{dr}} - \bar{z}_{n,V}^{\text{dr}})^\top.$$

The fixed-location doubly robust mean-embedding statistic, abbreviated DR-ME, is

$$\hat{\lambda}_{n,V}^{\text{dr}} := n \bar{z}_{n,V}^{\text{dr}\top} (S_{n,V}^{\text{dr}} + \gamma_n I_J)^{-1} \bar{z}_{n,V}^{\text{dr}}, \quad \gamma_n \downarrow 0. \quad (4)$$

This is the observed-data analogue of the finite-location Hotelling statistic.

For the following result, assume cross-fitted or independent-split nuisances, estimated propensities bounded away from zero, and fitted regressions uniformly bounded with probability tending to one. In K -fold notation, set $\alpha_{a,k} := \|\hat{\pi}_k(a | \cdot) - \pi_0(a | \cdot)\|_{L_2(P_X)}$ and $\beta_{a,k}(V) := \|\hat{m}_{a,k}(\cdot; V) - m_a(\cdot; V)\|_{L_2(P_X; \mathbb{R}^J)}$. We assume $\sum_{a=0}^1 \{\alpha_{a,k} + \beta_{a,k}(V)\} = o_p(1)$ and $\sum_{a=0}^1 \alpha_{a,k} \beta_{a,k}(V) = o_p(n^{-1/2})$. These are the standard consistency and product-rate conditions for orthogonal cross-fitted inference [4, 17].

Theorem 2.2 (Fixed-location first-order representation). *Fix $V \in \mathcal{Y}^J$, and let $\Sigma_V := \text{Var}_{P_0}\{\psi_V(Z)\}$. Under the bounded-kernel, identification, and nuisance conditions above,*

$$\sqrt{n}(\bar{z}_{n,V}^{\text{dr}} - \mu_V) = \frac{1}{\sqrt{n}} \sum_{i=1}^n \psi_V(Z_i) + o_p(1), \quad S_{n,V}^{\text{dr}} \rightarrow_p \Sigma_V.$$

If, in addition, Σ_V is positive definite and $\gamma_n \downarrow 0$, then $(S_{n,V}^{\text{dr}} + \gamma_n I_J)^{-1} \rightarrow_p \Sigma_V^{-1}$.

The proof is given in Appendix C. The theorem reduces the feasible fixed-location statistic to the empirical mean of the canonical gradient. Thus Σ_V is not merely a sample covariance used for numerical normalization; it is the observed-data covariance that enters the efficient local testing experiment developed next.

3 Efficient local testing geometry

We now study the fixed-location test $H_{0,V} : \mu_V = 0$ against $H_{1,V} : \mu_V \neq 0$, in the local regime where alternatives approach the null at $n^{-1/2}$ rate. This is the regime in which asymptotic power is nondegenerate: fixed alternatives are detected with probability tending to one, while faster local alternatives are invisible to regular tests. Appendix B recalls the local-asymptotic testing tools used below, including local asymptotic normality (LAN), contiguity, regular procedures, and the efficiency interpretation.

Let \mathcal{P} be the nonparametric model for the observed-data law on $\mathcal{Z} = \mathcal{X} \times \{0, 1\} \times \mathcal{Y}$, and fix $P_0 \in \mathcal{P}$ with $\mu_V(P_0) = 0$. Let T_{P_0} denote the tangent space at P_0 [2, 36]. For a score direction $g \in T_{P_0}$, let $t \mapsto P_{t,g}$ be a quadratic-mean differentiable regular path through P_0 with score g , and define the contiguous local alternatives

$$P_{n,h,g} := P_{h/\sqrt{n},g}^{\otimes n}, \quad h \in \mathbb{R}.$$

Quadratic-mean differentiability is the smoothness condition on this local submodel: the square-root likelihood is differentiable in $L_2(P_0)$ with derivative g . For i.i.d. experiments, this implies the LAN expansion and contiguity of $P_{n,h,g}$ with respect to $P_0^{\otimes n}$ [36, Theorem 7.2]; no other local likelihood regularity is used below. We use the same path to measure how the finite witness moves under a local alternative. Since Proposition 2.1 identifies ψ_V as the canonical gradient of μ_V , define the local drift

$$\eta_V(g) := \left. \frac{d}{dt} \right|_{t=0} \mu_V(P_{t,g}) = \mathbb{E}_{P_0} \{ \psi_V(Z) g(Z) \}. \quad (5)$$

Its covariance-whitened magnitude is

$$\lambda_V(g) := \eta_V(g)^\top \Sigma_V^{-1} \eta_V(g), \quad \Sigma_V := \text{Var}_{P_0} \{ \psi_V(Z) \}. \quad (6)$$

Thus $\eta_V(g)$ records how the selected witness coordinates move under the local alternative, while $\lambda_V(g)$ measures the size of that movement after normalization by the canonical-gradient covariance. If $\eta_V(g) = 0$, the selected locations are locally blind to g ; if $\eta_V(g) \neq 0$, the local alternative produces a first-order shift in the finite witness coordinates.

Theorem 3.1 (Efficient local testing geometry). *Fix $V \in \mathcal{Y}^J$ and let $P_0 \in \mathcal{P}$ satisfy $\mu_V(P_0) = 0$. Let $t \mapsto P_{t,g}$ be a quadratic-mean differentiable regular path through P_0 with score $g \in T_{P_0}$. Assume $\Sigma_V \succ 0$, $\gamma_n \downarrow 0$, and that the first-order representation and covariance consistency in Theorem 2.2 hold under $P_0^{\otimes n}$. Then, under $P_{n,h,g}$,*

$$\sqrt{n} \bar{z}_{n,V}^{\text{dr}} \xrightarrow{d} N(h\eta_V(g), \Sigma_V), \quad \hat{\lambda}_{n,V}^{\text{dr}} \xrightarrow{d} \chi_J^2(h^2\lambda_V(g)).$$

The proof is given in Appendix D. The theorem identifies the finite-signal Gaussian experiment induced by the finite-location causal null. Since ψ_V is the canonical gradient, the Hájek–Le Cam convolution theorem [36, Theorem 25.20] implies that any regular estimator T_n of μ_V with limit law $\sqrt{n}\{T_n - \mu_V(P_0)\} \xrightarrow{d} L$ has $L = N(0, \Sigma_V) * M$ for some noise law M , while $\bar{z}_{n,V}^{\text{dr}}$ attains the no-extra-noise case $M = \delta_0$. Thus Σ_V is the efficient covariance of the finite-signal limit experiment. For any contrast $a^\top \mu_V$, the squared local signal-to-noise ratio along g is $(a^\top \eta_V(g))^2 / (a^\top \Sigma_V a)$, whose supremum over $a \neq 0$ is $\lambda_V(g)$. The Hotelling statistic is the corresponding omnibus quadratic test in the whitened Gaussian shift experiment, with local power governed by $h^2\lambda_V(g)$. Appendix E gives additional details on this efficiency interpretation.

Remark 3.2 (Position relative to global MMD tests). The efficiency statement in Theorem 3.1 is a local testing statement for the regular finite signal μ_V . It is not a claim of optimality over all distributional alternatives. This differs from global MMD-type tests, which target a squared RKHS discrepancy such as $\|\Delta(P)\|_{\mathcal{H}_V}^2$. At the global null $\Delta(P_0) = 0$, the first-order derivative of this squared norm vanishes, so the ordinary Gaussian Wald geometry is replaced by a second-order, degenerate U -statistic or Gaussian-chaos null theory, as in the higher-order pathwise differentiability analysis of Luedtke et al. [22]. Recent doubly robust kernel tests for causal distributional effects similarly target global RKHS discrepancies and provide omnibus validity and power guarantees [6, 23, 40]. Our construction instead targets the finite projection

$\mu_V = L_V \Delta$, which remains first-order regular under the null. The tradeoff is explicit: a fixed finite V need not characterize every global alternative, but it yields interpretable witness coordinates, standard χ_J^2 calibration after sample splitting, and a covariance-whitened local-power criterion for learning where to test.

Remark 3.3 (Directional and omnibus benchmarks within the finite signal). Within the finite-signal Gaussian experiment, if the local direction g were known, the Neyman–Pearson linear test projects along $\Sigma_V^{-1} \eta_V(g)$. Equivalently, for scalar contrasts $a^\top \mu_V$, the squared local signal-to-noise ratio is

$$\frac{(a^\top \eta_V(g))^2}{a^\top \Sigma_V a},$$

whose supremum over $a \neq 0$ is $\eta_V(g)^\top \Sigma_V^{-1} \eta_V(g)$. When g is unknown, no uniformly most powerful test exists over all drift directions in the multivariate Gaussian shift experiment. The Hotelling statistic is the standard omnibus quadratic statistic in the whitened finite-signal experiment.

The noncentrality in Theorem 3.1 also explains how locations should be chosen. The relevant signal is not the raw Euclidean size of μ_V , but its size after whitening by the canonical-gradient covariance.

Proposition 3.4 (Local-power criterion for locations). *For fixed V , define*

$$\Lambda_V(P) := \mu_V(P)^\top \Sigma_V(P)^{-1} \mu_V(P),$$

where $\Sigma_V(P)$ is the covariance of the canonical gradient of μ_V at P . Suppose $\Sigma_V(P)$ is nonsingular in a neighborhood of P_0 and continuous along $t \mapsto P_{t,g}$. Then, along $P_{h/\sqrt{n},g}$,

$$\mu_V(P_{h/\sqrt{n},g}) = \frac{h}{\sqrt{n}} \eta_V(g) + o(n^{-1/2}), \quad n \Lambda_V(P_{h/\sqrt{n},g}) \rightarrow h^2 \lambda_V(g).$$

The proof is given in Appendix D. Proposition 3.4 links the population criterion for choosing V to the noncentrality parameter in Theorem 3.1. It also explains why an unwhitened witness norm is not the right learning objective: a large discrepancy in a high-variance direction may be weak for testing, while a smaller discrepancy in a low-noise direction may be more informative.

The unregularized quantity $\Lambda_V(P)$ is the asymptotic local-power object. In practice, our location learning uses a ridge-stabilized proxy,

$$\mathcal{P}_\tau(V) := \mu_V^\top (\Sigma_V + \tau I_J)^{-1} \mu_V, \quad \tau > 0, \tag{7}$$

which is numerically stable and approaches $\Lambda_V(P)$ as $\tau \downarrow 0$ whenever the covariance is uniformly nonsingular.

Finally, the fixed-location theory gives a direct route to valid testing when the locations are learned on data independent of the final test split.

Corollary 3.5 (Post-selection null law for split-sample locations). *Assume the global null $H_0 : \Delta = 0$. Let $\hat{V} \in \mathcal{V}$ be selected using data independent of the final testing split, and compute $\hat{\lambda}_{n_{\text{te}}, \hat{V}}^{\text{dr}}$ on that final split with $\gamma_{n_{\text{te}}} \downarrow 0$, using nuisance estimates independent of each test observation. Suppose that, conditionally on the learning split, the fixed-location first-order representation and covariance consistency of Theorem 2.2 hold at $V = \hat{V}$, with nondegenerate covariance; alternatively, suppose these conditions hold uniformly over $V \in \mathcal{V}$. Then, conditionally on the learning split,*

$$\hat{\lambda}_{n_{\text{te}}, \hat{V}}^{\text{dr}} \xrightarrow{d} \chi_{J,1-\alpha}^2.$$

Corollary 3.5 defines the split-sample DR-ME test. After learning \hat{V} on data independent of I_{te} , compute

$$p_{\text{te}}^{\text{dr}} := 1 - F_{\chi_{J,1-\alpha}^2}(\hat{\lambda}_{n_{\text{te}}, \hat{V}}^{\text{dr}}),$$

and reject the global null $H_0 : \Delta = 0$ at level α when

$$\hat{\lambda}_{n_{\text{te}}, \hat{V}}^{\text{dr}} > \chi_{J,1-\alpha}^2, \quad \text{equivalently} \quad p_{\text{te}}^{\text{dr}} \leq \alpha.$$

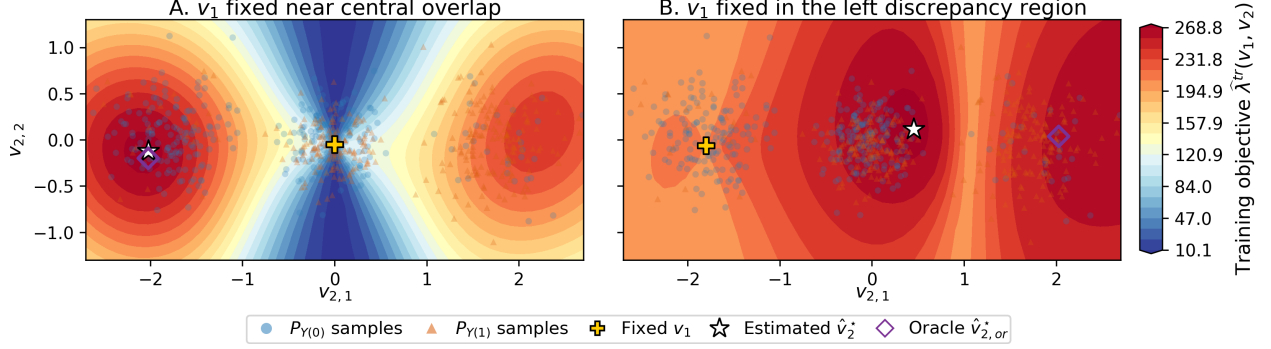


Figure 1: Training objective for learned causal locations. Each panel fixes v_1 and plots $v_2 \mapsto \hat{\mathcal{P}}_{\tau, \text{tr}}(v_1, v_2)$. Blue/orange points show samples from $P_{Y(0)}/P_{Y(1)}$; the gold marker is v_1 , the white star is the feasible maximizer, and the purple diamond is the oracle-nuisance maximizer on the same grid.

The reason this remains valid after learning is simple: $H_0 : \Delta = 0$ implies $\mu_V = 0$ for every V . Conditional on the learning split, \hat{V} is fixed relative to the final test data, so the fixed-location χ_J^2 calibration applies at $V = \hat{V}$. For a prespecified V , the same rule with \hat{V} replaced by V gives the fixed-location DR-ME test of $H_{0,V} : \mu_V = 0$, whose local power is governed by Theorem 3.1.

4 Learning locations by local power

Theorem 3.1 shows that fixed-location local power is governed by the witness after whitening by the efficient observed-data covariance. We therefore learn locations by maximizing

$$\mathcal{P}_\tau(V) := \mu_V^\top (\Sigma_V + \tau I_J)^{-1} \mu_V, \quad \tau > 0,$$

a ridge-stabilized version of the local-power criterion in Corollary 3.4. This follows the ME-test feature-learning principle [16], but uses the causal observed-data covariance geometry.

We split the sample as $I_\eta \cup I_{\text{tr}} \cup I_{\text{te}}$. Nuisances $\hat{\eta}$ are fitted on I_η , locations are learned on I_{tr} , and the final DR-ME test is computed on I_{te} . For $i \in I_{\text{tr}}$, let $\hat{z}_{i,V}^{\text{dr}} := z_V^{\text{dr}}(Z_i; \hat{\eta})$, with empirical mean and covariance $\bar{z}_{\text{tr},V}^{\text{dr}}$ and $S_{\text{tr},V}^{\text{dr}}$. The training objective is

$$\hat{\mathcal{P}}_{\tau, \text{tr}}(V) := \bar{z}_{\text{tr},V}^{\text{dr}\top} (S_{\text{tr},V}^{\text{dr}} + \tau I_J)^{-1} \bar{z}_{\text{tr},V}^{\text{dr}}. \quad (8)$$

Figure 1 illustrates this objective in a representative two-location example. For the learned output \hat{V} , define

$$\varepsilon_{\text{tr}}(\hat{V}) := \sup_{V \in \mathcal{V}} \hat{\mathcal{P}}_{\tau, \text{tr}}(V) - \hat{\mathcal{P}}_{\tau, \text{tr}}(\hat{V}).$$

This separates statistical error from numerical optimization error. It is zero for exhaustive finite-dictionary search, which is a natural set for non-Euclidean structured outcomes such as DNA or protein sequences [32, 37, 38]. In Euclidean classes, the assumptions below make $V \mapsto \hat{\mathcal{P}}_{\tau, \text{tr}}(V)$ Lipschitz, so a δ -net gives $\varepsilon_{\text{tr}}(\hat{V}) \leq \text{Lip}(\hat{\mathcal{P}}_{\tau, \text{tr}})\delta$; certified Lipschitz or branch-and-bound methods can also control the gap [12, 27, 33]. We keep $\varepsilon_{\text{tr}}(\hat{V})$ explicit because plain gradient ascent generally certifies stationarity, not global optimality [26].

Conditional on (I_η, I_{tr}) , the selected \hat{V} is fixed relative to I_{te} . Hence the final statistic computed on I_{te} is a fixed-location statistic at $V = \hat{V}$, and Corollary 3.5 gives post-selection calibration under the global null. The learning step affects power, not null calibration.

Theorem 4.1 (Uniform consistency of the learned criterion). *Assume $\mathcal{Y} \subset \mathbb{R}^d$ and let $\mathcal{V} \subset [-R, R]^{Jd}$ be compact. Let*

$$\Pi(\mathcal{V}) := \{v \in \mathbb{R}^d : v = v_j \text{ for some } V = (v_1, \dots, v_J) \in \mathcal{V}\}.$$

Suppose $k_Y(v, y)$ is uniformly bounded and Lipschitz in v over $\Pi(\mathcal{V})$, the estimated propensity is bounded away from zero with probability tending to one, and the fitted regressions $\hat{m}_a(x; v)$ are uniformly bounded and Lipschitz in v . Define $\rho_{n_\eta} := \sum_{a=0}^1 \left[\|\hat{\pi}(a | \cdot) - \pi_0(a | \cdot)\|_{L_2(P_X)} + \sup_{v \in \Pi(\mathcal{V})} \|\hat{m}_a(\cdot; v) - m_a(\cdot; v)\|_{L_2(P_X)} \right]$. If $n_\eta, n_{\text{tr}} \rightarrow \infty$ and $\rho_{n_\eta} = o_p(1)$, then, for fixed J ,

$$\Delta_{\text{tr}} := \sup_{V \in \mathcal{V}} \left| \hat{\mathcal{P}}_{\tau, \text{tr}}(V) - \mathcal{P}_\tau(V) \right| = O_p \left(\sqrt{\frac{Jd \log n_{\text{tr}}}{n_{\text{tr}}}} + \rho_{n_\eta} \right).$$

Consequently, for any output \hat{V} for which $\varepsilon_{\text{tr}}(\hat{V}) = O_p(e_{\text{tr}})$ and any $V_\tau^ \in \arg \max_{V \in \mathcal{V}} \mathcal{P}_\tau(V)$,*

$$\mathcal{P}_\tau(V_\tau^*) - \mathcal{P}_\tau(\hat{V}) = O_p \left(\sqrt{\frac{Jd \log n_{\text{tr}}}{n_{\text{tr}}}} + \rho_{n_\eta} + e_{\text{tr}} \right).$$

The proof is given in Appendix F. The first term is the statistical price of optimizing over a Jd -dimensional Euclidean class, the second is the nuisance-induced discrepancy, and the third is the empirical optimization gap. The theorem gives near-optimality within the chosen search class and for the ridge-stabilized criterion; it does not claim recovery of globally optimal locations over all of \mathcal{Y}^J .

For structured outcomes where Euclidean optimization is inappropriate, Appendix G gives a finite-dictionary analogue. If $\mathcal{C} = \{c_1, \dots, c_M\} \subset \mathcal{Y}$ and $\mathcal{V}_J(\mathcal{C}) \subset \mathcal{C}^J$, the Euclidean complexity term is replaced by $\sqrt{\frac{\log |\mathcal{V}_J(\mathcal{C})|}{n_{\text{tr}}}} \leq \sqrt{\frac{J \log M}{n_{\text{tr}}}}$. With exhaustive dictionary search, $\varepsilon_{\text{tr}}(\hat{V}) = 0$. Matrix formulas and implementation details are given in Appendix H.

5 Experiments

We evaluate three empirical claims in the main text. First, the proposed learned finite-location test is calibrated under observational confounding and is competitive with global doubly robust kernel tests, with higher power on localized distributional alternatives. Second, the efficient covariance geometry is important for learning informative locations, especially in structured or high-dimensional outcome spaces. Third, we illustrate the interpretability of the learned locations on a semi-synthetic medical imaging task based on MedMNIST [39]. Additional baselines, local noncentral- χ^2 diagnostics, runtime results are deferred to Appendix I and further validate the practical benefits of our approach.

All synthetic experiments use a confounded observational design with nonlinear outcome structure, three independent splits for nuisance fitting, location learning, and final testing, and 200 Monte Carlo replications at nominal level $\alpha = 0.05$. Nuisances are estimated from I_η , locations are learned from I_{tr} , and all reported tests are evaluated only on I_{te} . Unless stated otherwise, DR-ME uses a Gaussian outcome kernel, $M = 80$ candidate locations, and $J = 2$ selected locations. Full data-generating processes, nuisance models, bandwidth choices, and implementation details are given in Appendix I.

Calibration and power. Figure 2 compares DR-ME with finite-location diagnostics and the global kernel baseline. DR-ME-Rand uses the same statistic with random locations, IPW-ME uses only inverse-propensity weighting, DM-ME uses only the fitted regression contrast, Naive observed ME ignores the confounding X , and DR-ME-NoSplit learns and tests on the same data. DR-xKTE [23] is the calibrated global doubly robust kernel competitor. The left panel shows that calibration requires both orthogonalization and sample splitting: naive, plug-in, and no-split variants over-reject under the null in our confounded setting. The right panels show that, among calibrated methods (DR-ME, DR-xKTE, DR-ME-Rand), learning locations improves over random locations and even outperforms the global DR-xKTE baseline when the discrepancy is localized.

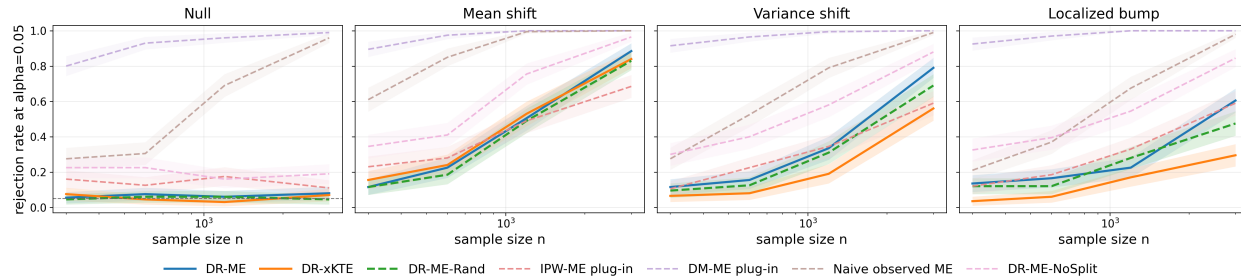


Figure 2: Calibration and power under observational confounding. Left: confounded null $P_{Y(0)} = P_{Y(1)}$. Right: mean-shift, variance-shift, and localized-bump alternatives. DR-ME is the most powerful test among calibrated ones (DR-ME, DR-xKTE, DR-ME-Rand) and even outperforms the global test DR-xKTE. DR-ME-Rand is calibrated but weaker, showing the benefits of learned locations. IPW-ME, DM-ME, Naive observed ME, and DR-ME-NoSplit over-reject under the null, so their high alternative rejection rates are not valid power.

Table 1: Non-scalar outcome two-bump ablation. Entries are rejection rates at level $\alpha = 0.05$. All methods use the same final DR-ME statistic; only the location-learning rule differs. Full covariance whitening remains calibrated under the null and gives the strongest power.

Method	Null				Two-bump alternative			
	$d_Y = 5$	10	25	50	$d_Y = 5$	10	25	50
Full whitening	0.070	0.025	0.050	0.070	0.940	0.945	0.760	0.660
Raw witness	0.055	0.035	0.070	0.055	0.135	0.210	0.380	0.500
Random	0.070	0.035	0.060	0.025	0.100	0.190	0.295	0.280

Covariance geometry. We next isolate the role of covariance whitening in location learning. The final test is fixed across variants: all use the same split-sample DR-ME Hotelling statistic on I_{te} ; only the training-split location criterion changes. We compare full whitening, $\hat{\mu}_V^\top (\hat{\Sigma}_V + \tau I)^{-1} \hat{\mu}_V$, with raw witness maximization, $\|\hat{\mu}_V\|^2$, and random locations. Outcomes are non-scalar, $Y \in \mathbb{R}^{d_Y}$, and the alternative places rare localized mass in two sparse regions, so most dictionary locations are uninformative. This tests whether whitening selects high signal-to-noise, nonredundant witness coordinates rather than large or random witness values. Table 1 shows that the difference is power, not calibration: all three rules are close to nominal level under the null, but full whitening is strongest at every dimension, with large gains when informative locations are rare. This supports the criterion $\mu_V^\top \Sigma_V^{-1} \mu_V$: covariance whitening selects finite-location coordinates with favorable observed-data signal-to-noise. Additional selection diagnostics are deferred to Appendix I.

Interpretable image outcomes on OCTMNIST. We include a qualitative semi-synthetic OCTMNIST experiment to illustrate localization on structured outcomes [39]. Synthetic covariates X drive both observational treatment assignment and heterogeneity, while OCTMNIST images are used only as image outcomes. Potential outcomes are full 28×28 OCT images $Y(a) = B + R(a)$, where B is sampled from normal OCT images and the residuals $R(0), R(1)$ are built from a synthetic DME-derived fluid-like template. The residual construction is mean-matched, with $\mathbb{E}\{R(1) - R(0) \mid X\} = 0$. Thus the treatment effect is primarily distributional: the treated law contains rare severe localized fluid-like deviations, while first-moment residual evidence is removed. Here, DR-ME learns with gradient based optimization a single image-space location on I_{tr} . Figure 3 shows that the learned location is not explained by an average residual shift: the oracle residual contrast is null, but v^* concentrates on the central fluid-like region. This illustrates the intended interpretability of finite-location testing: beyond rejecting a global distributional null, the method returns an outcome-space coordinate where the causal discrepancy is visible.

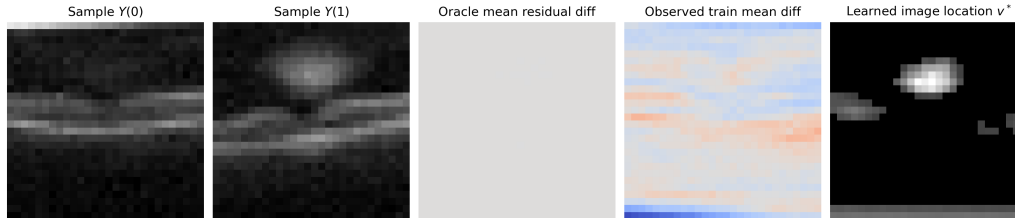


Figure 3: OCTMNIST image-location experiment. From left to right: sampled potential images $Y(0)$ and $Y(1)$, oracle residual mean difference, observed treated-versus-control training mean difference, and the learned image location v^* . The oracle residual mean contrast is blank by construction, while the observed training contrast can be nonzero due to confounding. The learned DR-ME location, selected on I_{tr} and evaluated on I_{te} , localizes the retinal region where the interventional image laws differ in distribution.

6 Discussion

This paper constructs a causal DR-ME Hotelling test for finite-location projections of interventional distributional discrepancies. For fixed locations, the target is a regular observed-data parameter whose canonical-gradient covariance gives the efficient local testing geometry. The resulting noncentrality $\eta_V(g)^\top \Sigma_V^{-1} \eta_V(g)$ controls local power and motivates the location-learning criterion. DR-ME is therefore complementary to global kernel tests: global tests target omnibus sensitivity, while DR-ME targets interpretable, locally efficient witness coordinates, with power depending on whether the learned locations capture the discrepancy. Natural extensions are threefold. First, the current theory treats point treatments under observed confounding; longitudinal, adaptive, missing-data, instrumental-variable, or proximal settings would require new canonical gradients and local experiments. Second, fixed kernels could be replaced by deep kernels or learned feature maps, when representation learning is separated from final testing to preserve calibration as we do. Third, location learning should exploit structure: finite dictionaries for non-Euclidean outcomes such as DNA sequences, and constrained or regularized search classes for images and other structured outputs.

Acknowledgements

Houssam Zenati and Arthur Gretton are supported by the Gatsby Charitable Foundation.

References

- [1] Heejung Bang and James M. Robins. Doubly robust estimation in missing data and causal inference models. *Biometrics*, 61(4):962–973, 2005. doi: 10.1111/j.1541-0420.2005.00377.x.
- [2] Peter J. Bickel, Chris A. J. Klaassen, Ya’acov Ritov, and Jon A. Wellner. *Efficient and Adaptive Estimation for Semiparametric Models*. Johns Hopkins University Press, 1993.
- [3] Victor Chernozhukov, Iván Fernández-Val, and Blaise Melly. Inference on counterfactual distributions. *Econometrica*, 81(6):2205–2268, 2013.
- [4] Victor Chernozhukov, Denis Chetverikov, Mert Demirer, Esther Duflo, Christian Hansen, Whitney Newey, and James Robins. Double/debiased machine learning for treatment and structural parameters. *The Econometrics Journal*, 21(1):C1–C68, 2018. doi: 10.1111/ectj.12097.
- [5] Kacper P Chwialkowski, Aaditya Ramdas, Dino Sejdinovic, and Arthur Gretton. Fast two-sample testing with analytic representations of probability measures. In *Advances in Neural Information Processing Systems*, volume 28, 2015.

- [6] Jake Fawkes, Robert Hu, Robin J. Evans, and Dino Sejdinovic. Doubly robust kernel statistics for testing distributional treatment effects. *Transactions on Machine Learning Research*, 2024.
- [7] William Fithian, Dennis Sun, and Jonathan Taylor. Optimal inference after model selection, 2014.
- [8] Thomas Gärtner. A survey of kernels for structured data. *ACM SIGKDD explorations newsletter*, 5(1): 49–58, 2003.
- [9] Arthur Gretton, Karsten M Borgwardt, Malte J Rasch, Bernhard Schölkopf, and Alexander Smola. A kernel two-sample test. *The Journal of Machine Learning Research*, 13(1):723–773, 2012.
- [10] Jinyong Hahn. On the role of the propensity score in efficient semiparametric estimation of average treatment effects. *Econometrica*, 66(2):315–331, 1998. doi: 10.2307/2998560.
- [11] Miguel A. Hernán and James M. Robins. *Causal Inference: What If*. Chapman & Hall/CRC, 2020.
- [12] Reiner Horst and Hoang Tuy. *Global Optimization: Deterministic Approaches*. Springer, Berlin, 3 edition, 1996.
- [13] Harold Hotelling. The generalization of student’s ratio. *The Annals of Mathematical Statistics*, 2(3): 360–378, 1931. doi: 10.1214/aoms/1177732979.
- [14] Aaron Hudson, Marco Carone, and Ali Shojaie. Inference on function-valued parameters using a restricted score test, 2021.
- [15] Guido W. Imbens and Donald B. Rubin. *Causal Inference for Statistics, Social, and Biomedical Sciences: An Introduction*. Cambridge University Press, 2015. doi: 10.1017/CBO9781139025751.
- [16] Wittawat Jitkrittum, Zoltán Szabó, Kacper P. Chwialkowski, and Arthur Gretton. Interpretable distribution features with maximum testing power. In *Advances in Neural Information Processing Systems 29*, pages 181–189, 2016.
- [17] Edward H. Kennedy. Semiparametric doubly robust targeted double machine learning: A review, 2022.
- [18] Daniel S. Kermany, Michael Goldbaum, Wenjia Cai, Carolina C. S. Valentim, Huiying Liang, Sally L. Baxter, Alex McKeown, Ge Yang, Xiaokang Wu, Fangbing Yan, Justin Dong, Made K. Prasadha, Jacqueline Pei, Magdalene Y. L. Ting, Jie Zhu, Christina Li, Sierra Hewett, Jason Dong, Ian Ziyar, Alexander Shi, Runze Zhang, Lianghong Zheng, Rui Hou, William Shi, Xiaogang Fu, Yaou Duan, Viet Anh Nguyen Huu, Cindy Wen, Edward D. Zhang, Chenyang L. Zhang, Oulan Li, Xiaobo Wang, Michael A. Singer, Xiaodong Sun, Jie Xu, Ali Tafreshi, M. Anthony Lewis, Huimin Xia, and Kang Zhang. Identifying medical diagnoses and treatable diseases by image-based deep learning. *Cell*, 172(5): 1122–1131.e9, 2018.
- [19] Arun Kumar Kuchibhotla, John E. Kolassa, and Todd A. Kuffner. Post-selection inference. *Annual Review of Statistics and Its Application*, 9:505–527, 2022. doi: 10.1146/annurev-statistics-100421-044639.
- [20] Lucien M. Le Cam and Grace Lo Yang. *Asymptotics in Statistics: Some Basic Concepts*. Springer Series in Statistics. Springer, 2 edition, 2000. doi: 10.1007/978-1-4612-1166-2.
- [21] Alex Luedtke and Incheoul Chung. One-step estimation of differentiable hilbert-valued parameters. *The Annals of Statistics*, 52(4):1534–1563, 2024.
- [22] Alexander R. Luedtke, Marco Carone, and Mark J. van der Laan. An omnibus non-parametric test of equality in distribution for unknown functions. *Journal of the Royal Statistical Society: Series B*, 81(1): 75–99, 2019.

- [23] Diego Martinez Taboada, Aaditya Ramdas, and Edward Kennedy. An efficient doubly-robust test for the kernel treatment effect. In *Advances in Neural Information Processing Systems*, volume 36, pages 59924–59952, 2023.
- [24] Krikamol Muandet, Motonobu Kanagawa, Sorawit Saengkyongam, and Sanparith Marukatat. Counterfactual mean embeddings. *Journal of Machine Learning Research*, 22(162):1–71, 2021.
- [25] Jerzy Neyman and Egon S. Pearson. On the problem of the most efficient tests of statistical hypotheses. *Philosophical Transactions of the Royal Society of London. Series A, Containing Papers of a Mathematical or Physical Character*, 231(694–706):289–337, 1933.
- [26] Jorge Nocedal and Stephen J. Wright. *Numerical Optimization*. Springer, New York, 2 edition, 2006.
- [27] S. A. Piyavskii. An algorithm for finding the absolute extremum of a function. *USSR Computational Mathematics and Mathematical Physics*, 12(4):57–67, 1972.
- [28] James M. Robins, Andrea Rotnitzky, and Lue Ping Zhao. Estimation of regression coefficients when some regressors are not always observed. *Journal of the American Statistical Association*, 89(427):846–866, 1994. doi: 10.1080/01621459.1994.10476818.
- [29] Paul R. Rosenbaum and Donald B. Rubin. The central role of the propensity score in observational studies for causal effects. *Biometrika*, 70(1):41–55, 1983. doi: 10.1093/biomet/70.1.41.
- [30] Christoph Rothe. Nonparametric estimation of distributional policy effects. *Journal of Econometrics*, 155(1):56–70, 2010.
- [31] Donald B. Rubin. Estimating causal effects of treatments in randomized and nonrandomized studies. *Journal of Educational Psychology*, 66(5):688–701, 1974. doi: 10.1037/h0037350.
- [32] Bernhard Schölkopf, Koji Tsuda, and Jean-Philippe Vert, editors. *Kernel Methods in Computational Biology*. MIT Press, Cambridge, MA, 2004. ISBN 9780262195096.
- [33] Bruno O. Shubert. A sequential method seeking the global maximum of a function. *SIAM Journal on Numerical Analysis*, 9(3):379–388, 1972.
- [34] Alex Smola, Arthur Gretton, Le Song, and Bernhard Schölkopf. A hilbert space embedding for distributions. In *International conference on algorithmic learning theory*, pages 13–31. Springer, 2007.
- [35] Bharath K Sriperumbudur, Kenji Fukumizu, and Gert RG Lanckriet. Universality, characteristic kernels and rkhs embedding of measures. *Journal of Machine Learning Research*, 12(7), 2011.
- [36] A. W. van der Vaart. *Asymptotic Statistics*, volume 3 of *Cambridge Series in Statistical and Probabilistic Mathematics*. Cambridge University Press, 1998. doi: 10.1017/CBO9780511802256.
- [37] Jean-Philippe Vert. Classification of biological sequences with kernel methods. In Yasubumi Sakakibara, Satoshi Kobayashi, Kengo Sato, Tetsuro Nishino, and Etsuji Tomita, editors, *Grammatical Inference: Algorithms and Applications*, volume 4201 of *Lecture Notes in Computer Science*, pages 7–18, Berlin, Heidelberg, 2006. Springer. doi: 10.1007/11872436_2.
- [38] Jean-Philippe Vert, Robert Thurman, and William S. Noble. Kernels for gene regulatory regions. In Yair Weiss, Bernhard Schölkopf, and John Platt, editors, *Advances in Neural Information Processing Systems 18*, pages 1401–1408, Cambridge, MA, 2005. MIT Press.
- [39] Jiancheng Yang, Rui Shi, Donglai Wei, Zequan Liu, Lin Zhao, Bilian Ke, Hanspeter Pfister, and Bingbing Ni. Medmnist v2-a large-scale lightweight benchmark for 2d and 3d biomedical image classification. *Scientific Data*, 10(1):41, 2023.

- [40] Houssam Zenati, Bariscan Bozkurt, and Arthur Gretton. Doubly-robust estimation of counterfactual policy mean embeddings. In *The Thirty-ninth Annual Conference on Neural Information Processing Systems*, 2025. URL <https://openreview.net/forum?id=0GD1X9JFf2>.
- [41] Houssam Zenati, Bariscan Bozkurt, and Arthur Gretton. Kernel treatment effects with adaptively collected data, 2025. URL <https://arxiv.org/abs/2510.10245>.

Appendix

Appendix organization. Appendix A collects notation and the full assumptions used in the main text. Appendix B gives a compact review of the local asymptotic tools used for the testing-efficiency statements. Appendix C proves the identification, canonical-gradient, and first-order representation results from Section 2. Appendix D proves the efficient local testing results from Section 3. Appendix E records auxiliary local-testing facts. Appendix F proves the Euclidean location-learning result from Section 4, and Appendix G gives the finite-dictionary variant for structured outcomes. Appendix H gives implementation details. Appendix I contains additional experiments.

An anonymized implementation is included in the supplementary material.

A Notation and full assumptions

Observed data and potential outcomes. We observe $Z = (X, A, Y) \sim P_0$, with binary treatment $A \in \{0, 1\}$. The potential outcomes are $Y(0), Y(1) \in \mathcal{Y}$. Unless a split-sample construction is explicitly used, $Z_1, \dots, Z_n \stackrel{\text{i.i.d.}}{\sim} P_0$.

Kernel and finite-location notation. The outcome kernel $k_Y : \mathcal{Y} \times \mathcal{Y} \rightarrow \mathbb{R}$ has RKHS \mathcal{H}_Y and feature map $\varphi_Y(y) = k_Y(\cdot, y)$. Throughout, k_Y is measurable, positive definite, and bounded: $\sup_y k_Y(y, y) \leq \kappa^2 < \infty$. For $V = (v_1, \dots, v_J) \in \mathcal{Y}^J$, write

$$k_V(y) := k_Y(V, y) := (k_Y(v_1, y), \dots, k_Y(v_J, y))^\top \in \mathbb{R}^J.$$

Interventional embeddings and witness coordinates. For $a \in \{0, 1\}$, let $\chi(a) := \mathbb{E}[\varphi_Y(Y(a))] \in \mathcal{H}_Y$, $\Delta := \chi(1) - \chi(0)$, and

$$w(y) := \langle \Delta, \varphi_Y(y) \rangle_{\mathcal{H}_Y} = \mathbb{E}[k_Y(y, Y(1))] - \mathbb{E}[k_Y(y, Y(0))].$$

The finite-location arm means and contrast are

$$\mu_{a,V} := \mathbb{E}[k_V(Y(a))], \quad \mu_V := \mu_{1,V} - \mu_{0,V} = (w(v_1), \dots, w(v_J))^\top \in \mathbb{R}^J.$$

Observed-data nuisance functions. For $a \in \{0, 1\}$, define

$$\pi_0(a | x) := P_0(A = a | X = x), \quad m_a(x; V) := \mathbb{E}[k_V(Y) | A = a, X = x].$$

A generic nuisance tuple is $\eta = (\pi, r_0, r_1)$, and the true tuple is $\eta_0 = (\pi_0, m_0, m_1)$.

Orthogonal pseudo-features. For $a \in \{0, 1\}$, define

$$\phi_V^a(Z; \eta) := \frac{\mathbf{1}\{A = a\}}{\pi(a | X)} \{k_V(Y) - r_a(X; V)\} + r_a(X; V), \quad z_V^{\text{dr}}(Z; \eta) := \phi_V^1(Z; \eta) - \phi_V^0(Z; \eta).$$

At the truth,

$$\psi_V(Z) := z_V^{\text{dr}}(Z; \eta_0) - \mu_V, \quad \Sigma_V := \text{Var}_{P_0}\{\psi_V(Z)\}.$$

Proposition 2.1 shows that ψ_V is the canonical gradient of μ_V in the observed-data model.

Fixed-location statistic. For fixed V , write the feasible pseudo-feature as

$$\hat{z}_{i,V}^{\text{dr}} := z_V^{\text{dr}}(Z_i; \hat{\eta}_{-i}),$$

where $\hat{\eta}_{-i}$ is trained on data independent of Z_i . This covers both K -fold cross-fitting and the independent test split used after location learning. Define

$$\bar{z}_{n,V}^{\text{dr}} := \frac{1}{n} \sum_{i=1}^n \hat{z}_{i,V}^{\text{dr}}, \quad S_{n,V}^{\text{dr}} := \frac{1}{n-1} \sum_{i=1}^n (\hat{z}_{i,V}^{\text{dr}} - \bar{z}_{n,V}^{\text{dr}})(\hat{z}_{i,V}^{\text{dr}} - \bar{z}_{n,V}^{\text{dr}})^\top.$$

The fixed-location Hotelling statistic is

$$\hat{\lambda}_{n,V}^{\text{dr}} := n \bar{z}_{n,V}^{\text{dr}\top} (S_{n,V}^{\text{dr}} + \gamma_n I_J)^{-1} \bar{z}_{n,V}^{\text{dr}}, \quad \gamma_n \downarrow 0.$$

Local asymptotic notation. Let \mathcal{P} be a semiparametric model for the observed-data law. For a fixed V , let $P_0 \in \mathcal{P}$ satisfy $\mu_V(P_0) = 0$, and let $T_{P_0} \subset L_2^0(P_0)$ be the tangent space. For a score direction $g \in T_{P_0}$, let $t \mapsto P_{t,g}$ be a regular quadratic-mean differentiable path through P_0 with score g , and define $P_{n,h,g} := P_{h/\sqrt{n},g}^{\otimes n}$. The local drift and whitened local signal are

$$\eta_V(g) := \left. \frac{d}{dt} \right|_{t=0} \mu_V(P_{t,g}) = \mathbb{E}_{P_0} \{\psi_V(Z)g(Z)\}, \quad \lambda_V(g) := \eta_V(g)^\top \Sigma_V^{-1} \eta_V(g).$$

Location learning notation. The full sample is split as $\{1, \dots, n\} = I_\eta \cup I_{\text{tr}} \cup I_{\text{te}}$, with $n_\eta = |I_\eta|$, $n_{\text{tr}} = |I_{\text{tr}}|$, and $n_{\text{te}} = |I_{\text{te}}|$. Nuisances are fitted on I_η , locations are learned on I_{tr} , and the final test is computed on I_{te} . The population and empirical ridge-stabilized criteria are

$$\mathcal{P}_\tau(V) := \mu_V^\top (\Sigma_V + \tau I_J)^{-1} \mu_V, \quad \hat{\mathcal{P}}_{\tau,\text{tr}}(V) := \bar{z}_{n_{\text{tr}},V}^{\text{dr}\top} (S_{n_{\text{tr}},V}^{\text{dr}} + \tau I_J)^{-1} \bar{z}_{n_{\text{tr}},V}^{\text{dr}}.$$

For a learned location set \hat{V} , define its empirical optimization gap

$$\varepsilon_{\text{tr}}(\hat{V}) := \sup_{V \in \mathcal{V}} \hat{\mathcal{P}}_{\tau,\text{tr}}(V) - \hat{\mathcal{P}}_{\tau,\text{tr}}(\hat{V}),$$

and the uniform learning error

$$\Delta_{\text{tr}} := \sup_{V \in \mathcal{V}} \left| \hat{\mathcal{P}}_{\tau,\text{tr}}(V) - \mathcal{P}_\tau(V) \right|.$$

Norms. Unless stated otherwise, $\|\cdot\|$ is the Euclidean norm, $\|\cdot\|_F$ is the Frobenius norm, and $\|\cdot\|_{L_2(P_X; \mathbb{R}^J)}$ is the $L_2(P_X)$ norm for \mathbb{R}^J -valued functions.

A.1 Observed-data identification

Assumption A.1 (Observed-data identification). For each $a \in \{0, 1\}$, the following hold.

- (i) *Consistency:* $Y = Y(a)$ whenever $A = a$.
- (ii) *Conditional exchangeability:* $Y(a) \perp A \mid X$.
- (iii) *Positivity:* there exists $\varepsilon > 0$ such that $\pi_0(a \mid X) \geq \varepsilon$ almost surely.

Under Assumption A.1, $\mu_{a,V} = \mathbb{E}[m_a(X; V)]$ and hence $\mu_V = \mathbb{E}[m_1(X; V) - m_0(X; V)]$.

A.2 Fixed-location nuisance and covariance conditions

Theorem 2.2 uses the following fixed-location conditions. They are stated for K -fold cross-fitting; for an independent nuisance split, remove the maxima over folds and use the single nuisance estimate $\hat{\eta}$.

Assumption A.2 (Fixed-location first-stage conditions). Fix $V \in \mathcal{Y}^J$. The validation folds $\mathcal{I}_1, \dots, \mathcal{I}_K$ satisfy $\min_k |\mathcal{I}_k|/n \geq c_K > 0$, with fixed K . For $i \in \mathcal{I}_k$, the nuisance estimate $\hat{\eta}_k = (\hat{\pi}_k, \hat{m}_{0,k}, \hat{m}_{1,k})$ is trained outside fold k .

There exist constants $\varepsilon > 0$ and $M < \infty$ such that, with probability tending to one,

$$\inf_{k,a,x} \hat{\pi}_k(a | x) \geq \varepsilon, \quad \sup_{k,a,x} \|\hat{m}_{a,k}(x; V)\| \leq M.$$

Moreover,

$$\max_k \sum_{a=0}^1 \left\{ \|\hat{\pi}_k(a | \cdot) - \pi_0(a | \cdot)\|_{L_2(P_X)} + \|\hat{m}_{a,k}(\cdot; V) - m_a(\cdot; V)\|_{L_2(P_X; \mathbb{R}^J)} \right\} = o_p(1),$$

and

$$\max_k \sum_{a=0}^1 \|\hat{\pi}_k(a | \cdot) - \pi_0(a | \cdot)\|_{L_2(P_X)} \|\hat{m}_{a,k}(\cdot; V) - m_a(\cdot; V)\|_{L_2(P_X; \mathbb{R}^J)} = o_p(n^{-1/2}).$$

Assumption A.3 (Nondegenerate fixed-location covariance). For the fixed location set V , the efficient covariance $\Sigma_V = \text{Var}_{P_0}\{\psi_V(Z)\}$ is positive definite.

Assumption A.3 is only needed for inverse-covariance whitening and chi-square limits. If Σ_V is singular, one may work in the nonzero eigenspace, but we do not pursue that extension.

A.3 Regular local paths

The local testing results are formulated along regular quadratic-mean differentiable paths. This is the primitive local smoothness condition; the LAN expansion used in the proofs follows from it.

Assumption A.4 (Regular QMD local path). For each fixed $g \in T_{P_0}$, there exists a path $t \mapsto P_{t,g} \subset \mathcal{P}$ through P_0 with densities $p_{t,g}$ relative to a dominating measure ν , such that

$$\int \left(\sqrt{p_{t,g}} - \sqrt{p_0} - \frac{t}{2} g \sqrt{p_0} \right)^2 d\nu = o(t^2).$$

Under Assumption A.4, the standard LAN expansion holds for $P_{n,h,g} = P_{h/\sqrt{n},g}^{\otimes n}$:

$$\log \frac{dP_{n,h,g}}{dP_0^{\otimes n}} = h \mathbb{G}_n g - \frac{1}{2} h^2 \|g\|_{L_2(P_0)}^2 + o_{P_0}(1), \quad \mathbb{G}_n g := \frac{1}{\sqrt{n}} \sum_{i=1}^n \{g(Z_i) - \mathbb{E}_{P_0} g(Z)\}.$$

It also implies contiguity of $P_{n,h,g}$ with respect to $P_0^{\otimes n}$. Thus $o_{P_0}(1)$ remainders in the fixed-location first-order expansion transfer to $o_{P_{n,h,g}}(1)$ remainders along the local path.

For Corollary 3.4, we additionally assume that $P \mapsto \Sigma_V(P)$ is continuous along $t \mapsto P_{t,g}$ at $t = 0$, and that $\Sigma_V(P_{t,g})$ remains nonsingular for t in a neighborhood of zero.

A.4 Euclidean location-learning conditions

Theorem 4.1 assumes $\mathcal{Y} \subset \mathbb{R}^d$ and a compact search class $\mathcal{V} \subset [-R, R]^J$. Let

$$\Pi(\mathcal{V}) := \{v \in \mathbb{R}^d : v = v_j \text{ for some } V = (v_1, \dots, v_J) \in \mathcal{V}\}.$$

Assumption A.5 (Euclidean location regularity). There exist constants $B_k, L_k, B_m, L_m < \infty$ such that the following hold.

(i) For all $v, v' \in \Pi(\mathcal{V})$ and $y \in \mathcal{Y}$,

$$|k_Y(v, y)| \leq B_k, \quad |k_Y(v, y) - k_Y(v', y)| \leq L_k \|v - v'\|.$$

(ii) With probability tending to one, for all $a \in \{0, 1\}$, $x \in \mathcal{X}$, and $v, v' \in \Pi(\mathcal{V})$,

$$|\hat{m}_a(x; v)| \leq B_m, \quad |\hat{m}_a(x; v) - \hat{m}_a(x; v')| \leq L_m \|v - v'\|.$$

(iii) The estimated propensity is uniformly bounded away from zero with probability tending to one:

$$\inf_{a, x} \hat{\pi}(a | x) \geq \underline{\varepsilon}$$

for some $\underline{\varepsilon} > 0$.

The true regressions $m_a(\cdot; v)$ inherit the boundedness and Lipschitz properties from the kernel by Jensen's inequality, so no separate smoothness assumption on m_a is needed for the learning theorem. The nuisance error entering Theorem 4.1 is

$$\rho_{n_\eta} := \sum_{a=0}^1 \left[\|\hat{\pi}(a | \cdot) - \pi_0(a | \cdot)\|_{L_2(P_X)} + \sup_{v \in \Pi(\mathcal{V})} \|\hat{m}_a(\cdot; v) - m_a(\cdot; v)\|_{L_2(P_X)} \right].$$

The learning theorem only requires $\rho_{n_\eta} = o_p(1)$, because it controls uniform consistency of the learning criterion rather than a root- n expansion of the final test statistic.

B Background on local asymptotic testing for fixed locations

This appendix reviews the local asymptotic tools used in Sections 2 and 3. Once the location set V is fixed, the target is the finite-dimensional parameter $\mu_V(P) \in \mathbb{R}^J$. Proposition 2.1 identifies its observed-data canonical gradient ψ_V , and Theorem 3.1 studies the local testing problem generated by this gradient.

The relevant objects are the local drift $\eta_V(g)$, the efficient covariance Σ_V , and the whitened local signal

$$\lambda_V(g) := \eta_V(g)^\top \Sigma_V^{-1} \eta_V(g).$$

The role of this appendix is to explain why these three quantities govern both regular estimation of μ_V and first-order local power of tests at the selected locations.

B.1 QMD paths and the local Gaussian approximation

The local theory is pathwise. We do not assume a finite-dimensional parametric model for the whole data-generating law. Instead, for each score direction $g \in T_{P_0}$, Assumption A.4 postulates a regular quadratic-mean differentiable path $t \mapsto P_{t,g}$ through P_0 . Quadratic mean differentiability means that, for densities $p_{t,g}$ relative to a dominating measure ν ,

$$\int \left(\sqrt{p_{t,g}} - \sqrt{p_0} - \frac{t}{2} g \sqrt{p_0} \right)^2 d\nu = o(t^2).$$

This condition is the standard local smoothness assumption behind Le Cam's asymptotic theory [2, 20, 36].

For the contiguous alternatives $P_{n,h,g} := P_{h/\sqrt{n},g}^{\otimes n}$, QMD implies the LAN expansion [36, Theorem 7.2]

$$\log \frac{dP_{n,h,g}}{dP_0^{\otimes n}} = h \mathbb{G}_n g - \frac{1}{2} h^2 \|g\|_{L_2(P_0)}^2 + o_{P_0}(1), \quad \mathbb{G}_n g := \frac{1}{\sqrt{n}} \sum_{i=1}^n g(Z_i),$$

where $g \in L_2^0(P_0)$. Thus, along each regular path, the original experiment is locally approximated by a Gaussian shift experiment. This is the only LAN input used in the paper. No least favorable submodel needs to be constructed for the main results; least favorable paths are useful for interpretation, but the proofs use arbitrary regular QMD paths and tangent-space projection.

B.2 Le Cam's third lemma and the local drift

Le Cam's third lemma describes how an asymptotically linear statistic shifts under a contiguous alternative. If

$$T_n = \frac{1}{\sqrt{n}} \sum_{i=1}^n \phi(Z_i) + o_{P_0}(1), \quad \mathbb{E}_{P_0} \phi(Z) = 0,$$

then, under $P_{n,h,g}$,

$$T_n \xrightarrow{d} N(h \mathbb{E}_{P_0} \{\phi(Z)g(Z)\}, \text{Var}_{P_0} \{\phi(Z)\}).$$

The covariance is unchanged to first order; the mean shifts in the direction correlated with the score g .

For the fixed-location statistic, $\phi = \psi_V$. Since ψ_V is the canonical gradient of μ_V , the pathwise derivative of μ_V along g is

$$\eta_V(g) := \left. \frac{d}{dt} \right|_{t=0} \mu_V(P_{t,g}) = \mathbb{E}_{P_0} \{\psi_V(Z)g(Z)\}.$$

Thus $\eta_V(g)$ is not an auxiliary definition. It is exactly the mean shift of the canonical-gradient statistic. If $\eta_V(g) = 0$, the selected locations are locally blind to direction g ; if $\eta_V(g) \neq 0$, the local alternative produces a first-order shift in the witness coordinates.

B.3 Regularity, convolution, and the efficient finite-signal experiment

In the nonparametric observed-data model, the canonical gradient of the finite signal μ_V is unique. Thus the efficiency statement is not a nontrivial comparison among different regular influence functions for the same target. Rather, it is a statement about the efficient limit experiment for regular estimation of μ_V .

By the Hájek–Le Cam convolution theorem [36, Theorem 25.20], if T_n is any regular estimator of μ_V and

$$\sqrt{n}\{T_n - \mu_V(P_0)\} \xrightarrow{d} L \quad \text{under } P_0^{\otimes n},$$

then

$$L = N(0, \Sigma_V) * M$$

for some probability law M . The canonical-gradient estimator $\bar{z}_{n,V}^{\text{dr}}$ attains the no-extra-noise case $M = \delta_0$, since Theorem 2.2 gives

$$\sqrt{n}(\bar{z}_{n,V}^{\text{dr}} - \mu_V) = \frac{1}{\sqrt{n}} \sum_{i=1}^n \psi_V(Z_i) + o_p(1).$$

Hence $N(0, \Sigma_V)$ is the efficient Gaussian limit for the finite witness. The covariance Σ_V is therefore not one possible normalization among many; it is the covariance of the efficient finite-signal experiment.

B.4 From efficient estimation to local testing geometry

Under Theorem 2.2 and the local path assumptions,

$$\sqrt{n} \bar{z}_{n,V}^{\text{dr}} \xrightarrow{d} N(h\eta_V(g), \Sigma_V) \quad \text{under } P_{n,h,g}.$$

After whitening, the efficient finite-signal experiment is

$$\Sigma_V^{-1/2} \sqrt{n} \bar{z}_{n,V}^{\text{dr}} \xrightarrow{d} N(h\Sigma_V^{-1/2} \eta_V(g), I_J).$$

For any scalar contrast $a^\top \mu_V$, the efficient squared local signal-to-noise ratio along g is

$$\frac{(a^\top \eta_V(g))^2}{a^\top \Sigma_V a}.$$

If the local direction g were known, optimizing this quantity over $a \neq 0$ gives the Rayleigh quotient

$$\max_{a \neq 0} \frac{(a^\top \eta_V(g))^2}{a^\top \Sigma_V a} = \eta_V(g)^\top \Sigma_V^{-1} \eta_V(g) = \lambda_V(g),$$

with optimizer proportional to $\Sigma_V^{-1} \eta_V(g)$. This is the directional Neyman–Pearson benchmark in the finite-signal Gaussian experiment.

When the direction is unknown, no uniformly most powerful test exists over all drift directions in the multivariate Gaussian shift experiment. The natural omnibus reduction is the whitened problem $G \sim N(m, I_J)$, with $H_0 : m = 0$ and $H_1 : m \neq 0$. In this limit experiment, the likelihood-ratio, Wald, and score statistics all reduce to $\|G\|^2$. Transported back to the finite witness, this is the Hotelling statistic based on Σ_V^{-1} , with noncentrality $h^2 \lambda_V(g)$. This is why the population location-learning criterion is

$$\Lambda_V(P) := \mu_V(P)^\top \Sigma_V(P)^{-1} \mu_V(P),$$

and why the practical criterion uses $\mathcal{P}_\tau(V) = \mu_V^\top (\Sigma_V + \tau I_J)^{-1} \mu_V$.

B.5 Relation to existing semiparametric kernel inference

This paper uses kernel embeddings, but the local problem is different from global MMD testing with unknown nuisance functions. In the unknown-function MMD setting of Luedtke et al. [22], the squared MMD has a degenerate first-order derivative under the null, and valid testing requires a second-order U-statistic analysis. Here, for fixed V , the target $\mu_V \in \mathbb{R}^J$ is first-order pathwise differentiable. The null limit is therefore a finite-dimensional chi-square law rather than a degenerate infinite weighted chi-square limit.

The paper is also related to Hilbert-valued semiparametric one-step estimation. General Hilbert-valued theory shows that, when an efficient influence function exists, one-step estimators can achieve root- n Hilbert-norm inference; counterfactual kernel mean embeddings are a key example [21]. Our construction can be viewed as applying bounded linear evaluation maps to the interventional RKHS discrepancy, yielding a finite-dimensional parameter with canonical gradient ψ_V . The contribution here is not Hilbert-valued estimation per se, but the testing geometry induced by this finite projection and its use for interpretable location learning.

B.6 Why the orthogonal DR geometry is the relevant geometry

The regression contrast $m_1(X; V) - m_0(X; V)$ has mean μ_V . If m_0 and m_1 were known, its covariance could be smaller than Σ_V . That comparison, however, corresponds to an oracle problem in which nuisance regressions are given. It is not the observed-data semiparametric problem faced by a regular procedure using flexible nuisance estimates.

A feasible plug-in regression contrast is first-order sensitive to regression error. Without stronger nuisance conditions, it does not provide the stable local expansion needed for regular local testing. By contrast, the orthogonal pseudo-feature $z_V^{\text{dr}}(Z; \eta)$ is built from the canonical gradient. Theorem 2.2 gives

$$\sqrt{n}(\bar{z}_{n,V}^{\text{dr}} - \mu_V) = \frac{1}{\sqrt{n}} \sum_{i=1}^n \psi_V(Z_i) + o_p(1), \quad S_{n,V}^{\text{dr}} \rightarrow_p \Sigma_V.$$

Thus the fixed-location test enters the local Gaussian experiment with the efficient observed-data score ψ_V . Thus the fixed-location test enters the efficient finite-signal Gaussian experiment with drift $\eta_V(g)$ and covariance Σ_V . This is the covariance geometry used both for local testing and for location learning.

C Proofs for Section 2

Throughout this appendix, fix $V = (v_1, \dots, v_J) \in \mathcal{Y}^J$ and write

$$k_V(y) := k_Y(V, y) = (k_Y(v_1, y), \dots, k_Y(v_J, y))^\top \in \mathbb{R}^J.$$

We use $\|\cdot\|$ for the Euclidean norm on \mathbb{R}^J . Since k_Y is bounded and J is fixed,

$$B_V := \sup_{y \in \mathcal{Y}} \|k_V(y)\| < \infty.$$

Consequently, $\|m_a(x; V)\| \leq B_V$ for $a \in \{0, 1\}$ and all x . We prove the cross-fitted case. The independent split case is the same argument with a single validation split independent of the nuisance-fitting sample.

C.1 Identification

Proof of the identification claim. Fix $a \in \{0, 1\}$. By iterated expectation,

$$\mu_{a,V} = \mathbb{E}[k_V(Y(a))] = \mathbb{E}[\mathbb{E}\{k_V(Y(a)) \mid X\}].$$

Conditional exchangeability gives

$$\mathbb{E}\{k_V(Y(a)) \mid X\} = \mathbb{E}\{k_V(Y(a)) \mid A = a, X\},$$

and consistency gives $Y = Y(a)$ on $\{A = a\}$. Hence

$$\mathbb{E}\{k_V(Y(a)) \mid A = a, X\} = \mathbb{E}\{k_V(Y) \mid A = a, X\} = m_a(X; V).$$

Therefore $\mu_{a,V} = \mathbb{E}[m_a(X; V)]$, and subtracting the two arm-specific identities yields

$$\mu_V = \mu_{1,V} - \mu_{0,V} = \mathbb{E}\{m_1(X; V) - m_0(X; V)\}.$$

□

C.2 A basic doubly robust identity

Lemma C.1 (Doubly robust algebra). *Fix $a \in \{0, 1\}$, let $\eta = (\pi, r_0, r_1)$, and define*

$$D_a(Z; \eta) := \phi_V^a(Z; \eta) - \phi_V^a(Z; \eta_0), \quad \eta_0 = (\pi_0, m_0, m_1).$$

Then

$$\begin{aligned} D_a(Z; \eta) &= \left(1 - \frac{\mathbf{1}\{A = a\}}{\pi_0(a \mid X)}\right) \{r_a(X; V) - m_a(X; V)\} \\ &\quad + \mathbf{1}\{A = a\} \left\{ \frac{1}{\pi(a \mid X)} - \frac{1}{\pi_0(a \mid X)} \right\} \{k_V(Y) - r_a(X; V)\}, \end{aligned} \quad (9)$$

and

$$P_0 D_a(\cdot; \eta) = P_0 \left[\frac{\pi_0(a \mid X) - \pi(a \mid X)}{\pi(a \mid X)} \{m_a(X; V) - r_a(X; V)\} \right]. \quad (10)$$

Moreover, on any event on which $\pi(a \mid X) \geq \underline{\pi} > 0$ almost surely and $\sup_x \|r_a(x; V)\| \leq M$,

$$P_0 \|D_a(\cdot; \eta)\|^2 \leq C \left\{ \|r_a(\cdot; V) - m_a(\cdot; V)\|_{L_2(P_X; \mathbb{R}^J)}^2 + \|\pi(a \mid \cdot) - \pi_0(a \mid \cdot)\|_{L_2(P_X)}^2 \right\}, \quad (11)$$

where $C < \infty$ depends only on the true positivity constant, $\underline{\pi}$, B_V , and M .

Proof. Write $I_a := \mathbf{1}\{A = a\}$, $\pi_a(X) := \pi(a \mid X)$, and $\pi_{0,a}(X) := \pi_0(a \mid X)$. Then

$$\begin{aligned} D_a(Z; \eta) &= \frac{I_a}{\pi_a(X)} \{k_V(Y) - r_a(X; V)\} + r_a(X; V) \\ &\quad - \frac{I_a}{\pi_{0,a}(X)} \{k_V(Y) - m_a(X; V)\} - m_a(X; V) \\ &= I_a \left\{ \frac{1}{\pi_a(X)} - \frac{1}{\pi_{0,a}(X)} \right\} \{k_V(Y) - r_a(X; V)\} \\ &\quad + \left(1 - \frac{I_a}{\pi_{0,a}(X)}\right) \{r_a(X; V) - m_a(X; V)\}, \end{aligned}$$

which proves (9).

Taking conditional expectation given X , the second term in (9) has mean zero. Also,

$$\mathbb{E}[I_a\{k_V(Y) - r_a(X; V)\} | X] = \pi_{0,a}(X)\{m_a(X; V) - r_a(X; V)\}.$$

Thus

$$\mathbb{E}\{D_a(Z; \eta) | X\} = \frac{\pi_{0,a}(X) - \pi_a(X)}{\pi_a(X)}\{m_a(X; V) - r_a(X; V)\},$$

and (10) follows.

For the L_2 bound, use $(u + v)^2 \leq 2u^2 + 2v^2$ in (9). True positivity implies

$$\mathbb{E}\left[\left|1 - \frac{I_a}{\pi_{0,a}(X)}\right|^2 \middle| X\right] \leq C,$$

so the first squared term is bounded by

$$C \|r_a(\cdot; V) - m_a(\cdot; V)\|_{L_2(P_X; \mathbb{R}^J)}^2.$$

On the stated event,

$$\left|\frac{1}{\pi_a(X)} - \frac{1}{\pi_{0,a}(X)}\right| \leq C|\pi_a(X) - \pi_{0,a}(X)|, \quad \|k_V(Y) - r_a(X; V)\| \leq B_V + M.$$

Hence the second squared term is bounded by

$$C \|\pi(a | \cdot) - \pi_0(a | \cdot)\|_{L_2(P_X)}^2.$$

Combining the two bounds proves (11). □

C.3 Proof of Proposition 2.1

Proof of Proposition 2.1. The bias identity is exactly (10). Since

$$\mathbb{E}\{\phi_V^a(Z; \eta)\} - \mu_{a,V} = P_0 D_a(\cdot; \eta),$$

we obtain

$$\mathbb{E}\{\phi_V^a(Z; \eta)\} - \mu_{a,V} = \mathbb{E}\left[\frac{\pi_0(a | X) - \pi(a | X)}{\pi(a | X)}\{m_a(X; V) - r_a(X; V)\}\right].$$

Therefore $\mathbb{E}\{\phi_V^a(Z; \eta)\} = \mu_{a,V}$ if either $\pi(a | \cdot) = \pi_0(a | \cdot)$ or $r_a(\cdot; V) = m_a(\cdot; V)$. Subtracting the two arm-specific identities gives the corresponding double-robustness statement for z_V^{dr} .

It remains to identify the canonical gradient. We prove the arm-specific statement; the contrast follows by linearity. Consider a regular path $t \mapsto P_t$ through P_0 with score $s \in T_{P_0}$. Write

$$m_{a,t}(x; V) := \mathbb{E}_t[k_V(Y) | A = a, X = x], \quad \mu_{a,V}(P_t) := \mathbb{E}_t[m_{a,t}(X; V)].$$

Let $s_X(X) := \mathbb{E}[s(Z) | X]$. Standard conditional-score calculus gives

$$\frac{d}{dt}\bigg|_{t=0} \mu_{a,V}(P_t) = \mathbb{E}[m_a(X; V)s_X(X)] + \mathbb{E}[\mathbb{E}\{(k_V(Y) - m_a(X; V))s(Z) | A = a, X\}].$$

The first term can be written as

$$\mathbb{E}[m_a(X; V)s_X(X)] = \mathbb{E}[\{m_a(X; V) - \mu_{a,V}\}s(Z)],$$

because $\mathbb{E}[s(Z)] = 0$. The second term can be represented in observed-data form as

$$\mathbb{E} \left[\frac{\mathbf{1}\{A = a\}}{\pi_0(a | X)} \{k_V(Y) - m_a(X; V)\} s(Z) \right].$$

Hence

$$\left. \frac{d}{dt} \right|_{t=0} \mu_{a,V}(P_t) = \mathbb{E} \left[\left\{ \frac{\mathbf{1}\{A = a\}}{\pi_0(a | X)} \{k_V(Y) - m_a(X; V)\} + m_a(X; V) - \mu_{a,V} \right\} s(Z) \right].$$

Thus the arm-specific canonical gradient is

$$\phi_V^a(Z; \eta_0) - \mu_{a,V}.$$

Since $\mu_V = \mu_{1,V} - \mu_{0,V}$, the canonical gradient of μ_V is

$$\{\phi_V^1(Z; \eta_0) - \mu_{1,V}\} - \{\phi_V^0(Z; \eta_0) - \mu_{0,V}\} = z_V^{\text{dr}}(Z; \eta_0) - \mu_V = \psi_V(Z).$$

□

C.4 Proof of Theorem 2.2

Proof of Theorem 2.2. Let $\mathcal{I}_1, \dots, \mathcal{I}_K$ be the validation folds, let $n_k := |\mathcal{I}_k|$, and let $P_{n,k}$ denote the empirical measure on fold k . For $i \in \mathcal{I}_k$, write

$$\hat{z}_i := z_V^{\text{dr}}(Z_i; \hat{\eta}_k), \quad z_0(Z_i) := z_V^{\text{dr}}(Z_i; \eta_0), \quad \psi_V(Z_i) = z_0(Z_i) - \mu_V.$$

Because K is fixed, all $o_p(\cdot)$ statements below may be read uniformly over k .

Let \mathcal{E}_n be the event on which the fitted propensities are uniformly bounded away from zero and the fitted regressions are uniformly bounded, as required by Assumption A.2. Then $P_0(\mathcal{E}_n) \rightarrow 1$. On this event, define

$$d_{a,k}(Z) := \phi_V^a(Z; \hat{\eta}_k) - \phi_V^a(Z; \eta_0), \quad d_k(Z) := d_{1,k}(Z) - d_{0,k}(Z),$$

and

$$\alpha_{a,k} := \|\hat{\pi}_k(a | \cdot) - \pi_0(a | \cdot)\|_{L_2(P_X)}, \quad \beta_{a,k} := \|\hat{m}_{a,k}(\cdot; V) - m_a(\cdot; V)\|_{L_2(P_X; \mathbb{R}^J)}.$$

By Lemma C.1 and Cauchy–Schwarz,

$$\|P_0 d_k\| \leq C \sum_{a=0}^1 \alpha_{a,k} \beta_{a,k}, \tag{12}$$

$$P_0 \|d_k\|^2 \leq C \sum_{a=0}^1 (\alpha_{a,k}^2 + \beta_{a,k}^2). \tag{13}$$

The assumed nuisance consistency and product-rate conditions therefore imply, uniformly over k ,

$$\|P_0 d_k\| = o_p(n^{-1/2}), \quad P_0 \|d_k\|^2 = o_p(1).$$

First-order expansion. Since

$$\bar{z}_{n,V}^{\text{dr}} = \sum_{k=1}^K \frac{n_k}{n} P_{n,k}(z_0 + d_k),$$

we have

$$\sqrt{n}(\bar{z}_{n,V}^{\text{dr}} - \mu_V) = \frac{1}{\sqrt{n}} \sum_{i=1}^n \psi_V(Z_i) + R_{1n} + R_{2n},$$

where

$$R_{1n} := \sqrt{n} \sum_{k=1}^K \frac{n_k}{n} (P_{n,k} - P_0) d_k, \quad R_{2n} := \sqrt{n} \sum_{k=1}^K \frac{n_k}{n} P_0 d_k.$$

For R_{2n} , (12) and the product-rate condition give

$$\|R_{2n}\| \leq C \sqrt{n} \sum_{k=1}^K \frac{n_k}{n} \sum_{a=0}^1 \alpha_{a,k} \beta_{a,k} = o_p(1).$$

For R_{1n} , condition on the training data used to construct $\hat{\eta}_k$. Then d_k is fixed and independent of the validation observations in fold k , so

$$\mathbb{E}_0 \left[\left\| \sqrt{n} \frac{n_k}{n} (P_{n,k} - P_0) d_k \right\|^2 \middle| \hat{\eta}_k \right] \leq \frac{n_k}{n} P_0 \|d_k\|^2 \leq P_0 \|d_k\|^2 = o_p(1).$$

A conditional Markov inequality gives each fold contribution as $o_p(1)$. Since K is fixed, $R_{1n} = o_p(1)$. Hence

$$\sqrt{n}(\bar{z}_{n,V}^{\text{dr}} - \mu_V) = \frac{1}{\sqrt{n}} \sum_{i=1}^n \psi_V(Z_i) + o_p(1).$$

Covariance consistency. Let

$$M_n := \frac{1}{n} \sum_{i=1}^n \hat{z}_i \hat{z}_i^\top, \quad M_0 := P_0 [z_0 z_0^\top].$$

The ordinary law of large numbers gives

$$\frac{1}{n} \sum_{i=1}^n z_0(Z_i) z_0(Z_i)^\top \rightarrow_p M_0,$$

because z_0 is bounded under the bounded-kernel and positivity assumptions. It remains to show that replacing $z_0(Z_i)$ by \hat{z}_i is negligible. Define

$$A_n := \frac{1}{n} \sum_{i=1}^n \|\hat{z}_i - z_0(Z_i)\|^2 = \sum_{k=1}^K \frac{n_k}{n} P_{n,k} \|d_k\|^2.$$

Conditionally on the nuisance fits,

$$\mathbb{E}_0[A_n \mid \hat{\eta}_1, \dots, \hat{\eta}_K] = \sum_{k=1}^K \frac{n_k}{n} P_0 \|d_k\|^2 = o_p(1),$$

so $A_n = o_p(1)$ by conditional Markov. Therefore,

$$\begin{aligned} \left\| M_n - \frac{1}{n} \sum_{i=1}^n z_0(Z_i) z_0(Z_i)^\top \right\|_F &\leq A_n + 2A_n^{1/2} \left(\frac{1}{n} \sum_{i=1}^n \|z_0(Z_i)\|^2 \right)^{1/2} \\ &= o_p(1). \end{aligned}$$

Thus $M_n \rightarrow_p M_0$. Since the first-order expansion implies $\bar{z}_{n,V}^{\text{dr}} \rightarrow_p \mu_V$,

$$S_{n,V}^{\text{dr}} = \frac{n}{n-1} \{M_n - \bar{z}_{n,V}^{\text{dr}} \bar{z}_{n,V}^{\text{dr}\top}\} \rightarrow_p M_0 - \mu_V \mu_V^\top = \text{Var}_{P_0} \{z_V^{\text{dr}}(Z; \eta_0)\} = \Sigma_V.$$

If Σ_V is positive definite and $\gamma_n \downarrow 0$, then

$$S_{n,V}^{\text{dr}} + \gamma_n I_J \rightarrow_p \Sigma_V,$$

and continuity of matrix inversion at positive definite matrices gives

$$(S_{n,V}^{\text{dr}} + \gamma_n I_J)^{-1} \rightarrow_p \Sigma_V^{-1}.$$

□

D Proofs for Section 3

Throughout this appendix, $V \in \mathcal{Y}^J$ is fixed and $P_0 \in \mathcal{P}$ satisfies

$$\mu_V(P_0) = 0.$$

Let $t \mapsto P_{t,g}$ be a quadratic-mean differentiable regular path through P_0 with score $g \in T_{P_0}$, and let

$$P_{n,h,g} := P_{h/\sqrt{n},g}^{\otimes n}.$$

By the standard QMD-to-LAN implication for i.i.d. experiments [36, Theorem 7.2],

$$\ell_{n,h,g} := \log \frac{dP_{n,h,g}}{dP_0^{\otimes n}} = h \mathbb{G}_n g - \frac{1}{2} h^2 \|g\|_{L_2(P_0)}^2 + o_{P_0}(1), \quad (14)$$

where

$$\mathbb{G}_n g := \frac{1}{\sqrt{n}} \sum_{i=1}^n g(Z_i),$$

and $P_{n,h,g}$ is contiguous with respect to $P_0^{\otimes n}$. Since $g \in T_{P_0} \subset L_2^0(P_0)$, $\mathbb{E}_{P_0}\{g(Z)\} = 0$.

D.1 A contiguity transfer lemma

Lemma D.1 (Contiguity transfer). *Let Q_n be contiguous with respect to $P_0^{\otimes n}$. If $R_n = o_{P_0}(1)$, then $R_n = o_{Q_n}(1)$. If $A_n \rightarrow_{P_0} A$, then $A_n \rightarrow_{Q_n} A$. In particular, if A is positive definite and $\gamma_n \downarrow 0$, then*

$$(A_n + \gamma_n I)^{-1} \rightarrow_{Q_n} A^{-1}.$$

Proof. For any $\epsilon > 0$,

$$P_0^{\otimes n}(\|R_n\| > \epsilon) \rightarrow 0.$$

Contiguity implies

$$Q_n(\|R_n\| > \epsilon) \rightarrow 0,$$

so $R_n = o_{Q_n}(1)$. The convergence $A_n \rightarrow A$ transfers by applying the same argument to the events

$$\{\|A_n - A\| > \epsilon\}.$$

Since $\gamma_n \downarrow 0$, $A_n + \gamma_n I \rightarrow_{Q_n} A$. The inverse statement follows from continuity of matrix inversion at positive definite matrices. □

D.2 Proof of Theorem 3.1

Proof of Theorem 3.1. Define

$$W_n := \frac{1}{\sqrt{n}} \sum_{i=1}^n \psi_V(Z_i).$$

Since $\mu_V(P_0) = 0$, the first-order representation in Theorem 2.2 gives, under $P_0^{\otimes n}$,

$$\sqrt{n} \bar{z}_{n,V}^{\text{dr}} = W_n + r_n, \quad r_n = o_{P_0}(1), \quad (15)$$

and

$$S_{n,V}^{\text{dr}} \rightarrow_{P_0} \Sigma_V.$$

By QMD, $P_{n,h,g}$ is contiguous with respect to $P_0^{\otimes n}$. Lemma D.1 therefore implies

$$r_n = o_{P_{n,h,g}}(1), \quad S_{n,V}^{\text{dr}} \rightarrow_{P_{n,h,g}} \Sigma_V, \quad (16)$$

and, since $\Sigma_V \succ 0$ and $\gamma_n \downarrow 0$,

$$(S_{n,V}^{\text{dr}} + \gamma_n I_J)^{-1} \rightarrow_{P_{n,h,g}} \Sigma_V^{-1}.$$

We next determine the local law of W_n . Under $P_0^{\otimes n}$, the joint vector

$$(W_n, \mathbb{G}_n g) = \left(\frac{1}{\sqrt{n}} \sum_{i=1}^n \psi_V(Z_i), \frac{1}{\sqrt{n}} \sum_{i=1}^n g(Z_i) \right)$$

converges by the multivariate central limit theorem to a centered Gaussian vector (W, G) with covariance

$$\begin{pmatrix} \Sigma_V & \eta_V(g) \\ \eta_V(g)^\top & \|g\|_{L_2(P_0)}^2 \end{pmatrix}.$$

Indeed,

$$\text{Cov}_{P_0} \{ \psi_V(Z), g(Z) \} = \mathbb{E}_{P_0} \{ \psi_V(Z) g(Z) \} = \eta_V(g).$$

Combining this joint central limit theorem with the LAN expansion (14), Le Cam's third lemma gives, under $P_{n,h,g}$,

$$W_n \xrightarrow{d} N(h\eta_V(g), \Sigma_V).$$

Together with (16), this yields

$$\sqrt{n} \bar{z}_{n,V}^{\text{dr}} \xrightarrow{d} N(h\eta_V(g), \Sigma_V) \quad \text{under } P_{n,h,g}.$$

For the quadratic statistic, write

$$\hat{\lambda}_{n,V}^{\text{dr}} = (\sqrt{n} \bar{z}_{n,V}^{\text{dr}})^\top (S_{n,V}^{\text{dr}} + \gamma_n I_J)^{-1} (\sqrt{n} \bar{z}_{n,V}^{\text{dr}}).$$

By Slutsky's theorem,

$$\hat{\lambda}_{n,V}^{\text{dr}} \xrightarrow{d} Y^\top \Sigma_V^{-1} Y, \quad Y \sim N(h\eta_V(g), \Sigma_V).$$

Equivalently, if $Z \sim N(0, I_J)$, then

$$Y = \Sigma_V^{1/2} Z + h\eta_V(g),$$

and therefore

$$Y^\top \Sigma_V^{-1} Y = \left\| Z + h \Sigma_V^{-1/2} \eta_V(g) \right\|^2.$$

Thus

$$\hat{\lambda}_{n,V}^{\text{dr}} \xrightarrow{d} \chi_J^2(h^2 \eta_V(g)^\top \Sigma_V^{-1} \eta_V(g)) = \chi_J^2(h^2 \lambda_V(g)).$$

The whitened representation follows from the same argument:

$$\Sigma_V^{-1/2} \sqrt{n} \bar{z}_{n,V}^{\text{dr}} \xrightarrow{d} N(h \Sigma_V^{-1/2} \eta_V(g), I_J),$$

and

$$\hat{\lambda}_{n,V}^{\text{dr}} = \left\| \Sigma_V^{-1/2} \sqrt{n} \bar{z}_{n,V}^{\text{dr}} \right\|^2 + o_{P_{n,h,g}}(1).$$

□

D.3 Proof of Proposition 3.4

Proof of Proposition 3.4. Let $t_n := h/\sqrt{n}$. Since μ_V is pathwise differentiable at P_0 along $t \mapsto P_{t,g}$, with derivative $\eta_V(g)$, and since $\mu_V(P_0) = 0$,

$$\mu_V(P_{t,g}) = t \eta_V(g) + o(t) \quad \text{as } t \rightarrow 0.$$

Substituting $t = t_n$ gives

$$\mu_V(P_{h/\sqrt{n},g}) = \frac{h}{\sqrt{n}} \eta_V(g) + o(n^{-1/2}).$$

Let

$$\Sigma_n := \Sigma_V(P_{t_n,g}).$$

By continuity along the path and nonsingularity in a neighborhood of P_0 ,

$$\Sigma_n \rightarrow \Sigma_V(P_0) = \Sigma_V, \quad \Sigma_n^{-1} \rightarrow \Sigma_V^{-1}.$$

Set

$$u_n := \sqrt{n} \mu_V(P_{t_n,g}).$$

Then

$$u_n = h \eta_V(g) + o(1).$$

Therefore

$$n \Lambda_V(P_{t_n,g}) = u_n^\top \Sigma_n^{-1} u_n \rightarrow h^2 \eta_V(g)^\top \Sigma_V^{-1} \eta_V(g) = h^2 \lambda_V(g).$$

□

D.4 Proof of Corollary 3.5

Proof of Corollary 3.5. Under the global null $H_0 : \Delta = 0$, every finite-location signal is zero:

$$\mu_V(P_0) = 0 \quad \text{for all } V \in \mathcal{Y}^J.$$

In particular, conditional on the learning split,

$$\mu_{\hat{V}}(P_0) = 0.$$

Conditional on the learning split, the selected \hat{V} is fixed relative to the final testing data. The final statistic is therefore a fixed-location statistic at $V = \hat{V}$, computed with $\gamma_{n_{\text{te}}} \downarrow 0$. By the assumed conditional fixed-location first-order representation and covariance consistency, together with the multivariate central limit theorem and Slutsky's theorem,

$$\hat{\lambda}_{n_{\text{te}}, \hat{V}}^{\text{dr}} \xrightarrow{d} \chi_J^2 \quad \text{conditionally on the learning split.}$$

Thus the conditional rejection probability converges to α at the chi-square critical value. Since the rejection indicator is bounded and the limiting rejection probability is nonrandom, the unconditional rejection probability also converges to α . □

E Additional local-theory refinements

Throughout this appendix, fix $V \in \mathcal{Y}^J$ and let $P_0 \in \mathcal{P}$ satisfy

$$\mu_V(P_0) = 0.$$

Write T_{P_0} for the tangent space at P_0 . For $g \in T_{P_0}$, let

$$P_{n,h,g} := P_{h/\sqrt{n},g}^{\otimes n}$$

denote the corresponding contiguous local alternatives. Recall that

$$\psi_V(Z) = z_V^{\text{dr}}(Z; \eta_0) - \mu_V$$

is the canonical gradient of the fixed-location signal μ_V , and define

$$\Sigma_V := \text{Var}_{P_0}\{\psi_V(Z)\}, \quad \eta_V(g) := \mathbb{E}_{P_0}\{\psi_V(Z)g(Z)\}, \quad \lambda_V(g) := \eta_V(g)^\top \Sigma_V^{-1} \eta_V(g).$$

The main text identifies the efficient finite-signal Gaussian experiment and the omnibus Hotelling statistic. This appendix records the corresponding known-direction benchmark, which explains the role of $\lambda_V(g)$ as a directional local signal-to-noise ratio.

E.1 Known-direction score benchmark

Theorem 3.1 treats the omnibus alternative $\mu_V \neq 0$. If the local direction g were known, the finite-signal Gaussian experiment also gives a one-dimensional Neyman–Pearson benchmark.

Corollary E.1 (Directional efficient score test). *Assume the conditions of Theorem 3.1, and suppose that $\eta_V(g) \neq 0$. Define*

$$L_{n,V,g} := \frac{\eta_V(g)^\top (S_{n,V}^{\text{dr}} + \gamma_n I_J)^{-1} \sqrt{n} z_{n,V}^{\text{dr}}}{\left[\eta_V(g)^\top (S_{n,V}^{\text{dr}} + \gamma_n I_J)^{-1} \eta_V(g) \right]^{1/2}}.$$

Then, under $P_0^{\otimes n}$,

$$L_{n,V,g} \xrightarrow{d} N(0, 1),$$

and, under $P_{n,h,g}$,

$$L_{n,V,g} \xrightarrow{d} N(h\sqrt{\lambda_V(g)}, 1).$$

Consequently, the one-sided level- α rule that rejects for

$$L_{n,V,g} > z_{1-\alpha}$$

has asymptotic power

$$1 - \Phi(z_{1-\alpha} - h\sqrt{\lambda_V(g)}).$$

Moreover, in the finite-signal Gaussian experiment

$$Y \sim N(h\eta_V(g), \Sigma_V), \quad h \in \mathbb{R},$$

this directional rule is Neyman–Pearson optimal for testing $h = 0$ against any fixed simple alternative $h = h_1 > 0$.

Proof. Let

$$A_n := (S_{n,V}^{\text{dr}} + \gamma_n I_J)^{-1}, \quad W_n := \sqrt{n} z_{n,V}^{\text{dr}}.$$

By Theorem 3.1,

$$W_n \xrightarrow{d} N(h\eta_V(g), \Sigma_V) \quad \text{under } P_{n,h,g},$$

and

$$A_n \rightarrow_p \Sigma_V^{-1}.$$

Therefore, by Slutsky's theorem,

$$\eta_V(g)^\top A_n W_n = \eta_V(g)^\top \Sigma_V^{-1} W_n + o_{P_{n,h,g}}(1).$$

Hence

$$\eta_V(g)^\top A_n W_n \xrightarrow{d} N(h\eta_V(g)^\top \Sigma_V^{-1} \eta_V(g), \eta_V(g)^\top \Sigma_V^{-1} \Sigma_V \Sigma_V^{-1} \eta_V(g)),$$

or equivalently,

$$\eta_V(g)^\top A_n W_n \xrightarrow{d} N(h\lambda_V(g), \lambda_V(g)).$$

Also,

$$\eta_V(g)^\top A_n \eta_V(g) \rightarrow_p \eta_V(g)^\top \Sigma_V^{-1} \eta_V(g) = \lambda_V(g).$$

Dividing numerator and denominator yields

$$L_{n,V,g} \xrightarrow{d} N(h\sqrt{\lambda_V(g)}, 1).$$

The null statement is obtained by setting $h = 0$, and the displayed power formula follows immediately.

For the Neyman–Pearson statement, in the finite-signal Gaussian experiment

$$Y \sim N(h\eta_V(g), \Sigma_V),$$

the log-likelihood ratio between $h = h_1$ and $h = 0$ is, up to an additive constant,

$$h_1 \eta_V(g)^\top \Sigma_V^{-1} Y - \frac{1}{2} h_1^2 \eta_V(g)^\top \Sigma_V^{-1} \eta_V(g).$$

Thus the most powerful level- α test rejects for large values of

$$\eta_V(g)^\top \Sigma_V^{-1} Y,$$

or equivalently for large values of its standardized version. This is the limiting test generated by $L_{n,V,g}$. \square

E.2 Interpretation

For any scalar contrast $a^\top \mu_V$, the squared local signal-to-noise ratio along g is

$$\frac{(a^\top \eta_V(g))^2}{a^\top \Sigma_V a}.$$

The known-direction benchmark optimizes this quantity over $a \neq 0$, yielding the Rayleigh quotient

$$\lambda_V(g) = \eta_V(g)^\top \Sigma_V^{-1} \eta_V(g).$$

When g is unknown, no uniformly most powerful test exists over all drift directions in the multivariate Gaussian shift experiment. The fixed-location DR-ME statistic instead uses the omnibus quadratic statistic in the whitened efficient Gaussian experiment, whose local power is governed by the same noncentrality $h^2 \lambda_V(g)$. This is why the population criterion

$$\Lambda_V(P) = \mu_V(P)^\top \Sigma_V(P)^{-1} \mu_V(P)$$

is the relevant target for learning informative locations.

F Proofs for Section 4

Throughout this appendix, write $n := n_{\text{tr}}$ and

$$D_\eta := \sigma((Z_i)_{i \in I_\eta}, \hat{\pi}, \hat{m}_0, \hat{m}_1).$$

For $V \in \mathcal{V}$ and $z = (x, a, y) \in \mathcal{Z}$, define the nuisance-fitted pseudo-feature

$$\hat{z}_V(z) := z_V^{\text{dr}}(z; \hat{\eta}), \quad \hat{\eta} = (\hat{\pi}, \hat{m}_0, \hat{m}_1).$$

Thus, for $i \in I_{\text{tr}}$, $\hat{z}_{i,V}^{\text{dr}} = \hat{z}_V(Z_i)$. Conditional on D_η , the variables $\{\hat{z}_V(Z_i) : i \in I_{\text{tr}}\}$ are i.i.d. for each fixed V .

Define the conditional population quantities

$$\mu_V^\eta := \mathbb{E}[\hat{z}_V(Z) \mid D_\eta], \quad M_V^\eta := \mathbb{E}[\hat{z}_V(Z)\hat{z}_V(Z)^\top \mid D_\eta], \quad \Sigma_V^\eta := M_V^\eta - \mu_V^\eta \mu_V^{\eta\top},$$

and the conditional criterion

$$\mathcal{P}_\tau^\eta(V) := \mu_V^{\eta\top} (\Sigma_V^\eta + \tau I_J)^{-1} \mu_V^\eta.$$

The proof of Theorem 4.1 uses

$$\sup_{V \in \mathcal{V}} |\hat{\mathcal{P}}_{\tau, \text{tr}}(V) - \mathcal{P}_\tau(V)| \leq \sup_{V \in \mathcal{V}} |\hat{\mathcal{P}}_{\tau, \text{tr}}(V) - \mathcal{P}_\tau^\eta(V)| + \sup_{V \in \mathcal{V}} |\mathcal{P}_\tau^\eta(V) - \mathcal{P}_\tau(V)|. \quad (17)$$

The first term is the training-split empirical fluctuation. The second term is the nuisance-induced discrepancy between the conditional and oracle population criteria.

F.1 Uniform bounds for pseudo-features

Let

$$\bar{\varepsilon} := \min\{\varepsilon, \underline{\varepsilon}\},$$

where ε is the true positivity constant and $\underline{\varepsilon}$ is the fitted-propensity lower bound in Assumption A.5.

Lemma F.1 (Uniform boundedness and Lipschitzness). *Under Assumption A.5, there exist finite constants*

$$B_z := 2\sqrt{J} \left[\bar{\varepsilon}^{-1}(B_k + B_m) + B_m \right], \quad L_z := 2 \left[\bar{\varepsilon}^{-1}(L_k + L_m) + L_m \right],$$

such that, with probability tending to one, for all $z \in \mathcal{Z}$ and all $V, V' \in \mathcal{V}$,

$$\|\hat{z}_V(z)\| \leq B_z, \quad \|\hat{z}_V(z) - \hat{z}_{V'}(z)\| \leq L_z \|V - V'\|.$$

The same bounds hold for the oracle feature $z_V^0(z) := z_V^{\text{dr}}(z; \eta_0)$.

Proof. For $V = (v_1, \dots, v_J)$,

$$\|k_V(y)\|^2 = \sum_{j=1}^J |k_Y(v_j, y)|^2 \leq JB_k^2, \quad \|\hat{m}_a(x; V)\|^2 \leq JB_m^2.$$

Hence the arm-specific fitted score is bounded by

$$\left\| \frac{\mathbf{1}\{A=a\}}{\hat{\pi}(a \mid X)} \{k_V(Y) - \hat{m}_a(X; V)\} + \hat{m}_a(X; V) \right\| \leq \sqrt{J} \left[\bar{\varepsilon}^{-1}(B_k + B_m) + B_m \right].$$

Subtracting the two arm-specific scores gives the bound for \hat{z}_V .

For Lipschitzness, Assumption A.5 gives

$$\|k_V(y) - k_{V'}(y)\| \leq L_k \|V - V'\|, \quad \|\hat{m}_a(x; V) - \hat{m}_a(x; V')\| \leq L_m \|V - V'\|.$$

Therefore each arm-specific fitted score is Lipschitz with constant

$$\bar{\varepsilon}^{-1}L_k + (\bar{\varepsilon}^{-1} + 1)L_m \leq \bar{\varepsilon}^{-1}(L_k + L_m) + L_m.$$

Subtracting the two arms gives the displayed L_z . The oracle feature satisfies the same bounds because the true regressions inherit boundedness and Lipschitzness from k_Y , and the true propensities are bounded below by ε . \square

F.2 Uniform empirical control

Lemma F.2 (Uniform concentration for bounded Lipschitz Euclidean classes). *Let $\mathcal{V} \subset [-R, R]^m$, and let*

$$\mathcal{F} := \{f_V : V \in \mathcal{V}\}$$

be a class of measurable real-valued functions such that, conditionally on D_η ,

$$|f_V(z)| \leq B, \quad |f_V(z) - f_{V'}(z)| \leq L\|V - V'\|$$

for all z and all V, V' . Then

$$\sup_{V \in \mathcal{V}} |(P_n^{\text{tr}} - P_0)f_V| = O_p\left(\sqrt{\frac{m \log n}{n}}\right),$$

where $P_n^{\text{tr}} := n^{-1} \sum_{i \in I_{\text{tr}}} \delta_{Z_i}$, and the hidden constant depends only on R, B, L, m .

Proof. Let \mathcal{N}_δ be a δ -net of \mathcal{V} . Since $\mathcal{V} \subset [-R, R]^m$,

$$|\mathcal{N}_\delta| \leq \left(\frac{C_0 R}{\delta}\right)^m$$

for a universal constant C_0 . For each V , choose $\Pi_\delta(V) \in \mathcal{N}_\delta$ with $\|V - \Pi_\delta(V)\| \leq \delta$. Then

$$\sup_{V \in \mathcal{V}} |(P_n^{\text{tr}} - P_0)f_V| \leq \max_{U \in \mathcal{N}_\delta} |(P_n^{\text{tr}} - P_0)f_U| + 2L\delta.$$

Conditionally on D_η , Hoeffding's inequality and a union bound give

$$\Pr\left(\max_{U \in \mathcal{N}_\delta} |(P_n^{\text{tr}} - P_0)f_U| > t \mid D_\eta\right) \leq 2|\mathcal{N}_\delta| \exp\left(-\frac{nt^2}{2B^2}\right).$$

Taking $\delta = n^{-1/2}$ and $t = M\sqrt{m \log n/n}$, with M large enough, proves the result. \square

Lemma F.3 (Uniform mean and covariance concentration). *Under Assumption A.5,*

$$\sup_{V \in \mathcal{V}} \|\bar{z}_{\text{tr}, V}^{\text{dr}} - \mu_V^\eta\| = O_p\left(\sqrt{\frac{Jd \log n}{n}}\right),$$

and, with

$$\widehat{M}_{\text{tr}, V} := \frac{1}{n} \sum_{i \in I_{\text{tr}}} \hat{z}_{i, V}^{\text{dr}} \hat{z}_{i, V}^{\text{dr}\top},$$

$$\sup_{V \in \mathcal{V}} \|\widehat{M}_{\text{tr}, V} - M_V^\eta\|_F = O_p\left(\sqrt{\frac{Jd \log n}{n}}\right).$$

Consequently,

$$\sup_{V \in \mathcal{V}} \|\mathcal{S}_{\text{tr}, V}^{\text{dr}} - \Sigma_V^\eta\|_F = O_p\left(\sqrt{\frac{Jd \log n}{n}}\right).$$

Proof. Set $m = Jd$. By Lemma F.1, each coordinate class

$$\{z \mapsto \hat{z}_{V, j}(z) : V \in \mathcal{V}\}$$

is conditionally bounded and Lipschitz. Applying Lemma F.2 coordinatewise and using fixed J yields the mean bound.

For second moments, apply the same lemma to

$$\{z \mapsto \hat{z}_{V,j}(z) \hat{z}_{V,\ell}(z) : V \in \mathcal{V}\}.$$

This class is conditionally bounded by B_z^2 and Lipschitz with constant $2B_z L_z$. Applying the scalar concentration bound entrywise and using fixed J gives the second-moment bound.

Finally,

$$S_{\text{tr},V}^{\text{dr}} = \frac{n}{n-1} \left(\widehat{M}_{\text{tr},V} - \bar{z}_{\text{tr},V}^{\text{dr}} \bar{z}_{\text{tr},V}^{\text{dr}\top} \right), \quad \Sigma_V^\eta = M_V^\eta - \mu_V^\eta \mu_V^{\eta\top}.$$

The uniform boundedness of $\bar{z}_{\text{tr},V}^{\text{dr}}$ and μ_V^η , together with

$$\|uu^\top - vv^\top\|_F \leq (\|u\| + \|v\|)\|u - v\|,$$

gives the covariance bound. □

F.3 Nuisance transfer

Lemma F.4 (Uniform nuisance transfer). *Under Assumption A.5,*

$$\sup_{V \in \mathcal{V}} \|\mu_V^\eta - \mu_V\| = O_p(\rho_{n_\eta}), \quad \sup_{V \in \mathcal{V}} \|\Sigma_V^\eta - \Sigma_V\|_F = O_p(\rho_{n_\eta}).$$

Proof. For $V \in \mathcal{V}$, write

$$z_V^0(Z) := z_V^{\text{dr}}(Z; \eta_0), \quad d_V(Z) := \hat{z}_V(Z) - z_V^0(Z).$$

Then $\mu_V^\eta - \mu_V = P_0 d_V$. For each arm a , let

$$D_{a,V}(Z) := \phi_V^a(Z; \hat{\eta}) - \phi_V^a(Z; \eta_0).$$

Lemma C.1 gives, uniformly in V ,

$$P_0 \|D_{a,V}\|^2 \leq C \left\{ \|\hat{\pi}(a | \cdot) - \pi_0(a | \cdot)\|_{L_2(P_X)}^2 + \|\hat{m}_a(\cdot; V) - m_a(\cdot; V)\|_{L_2(P_X; \mathbb{R}^J)}^2 \right\}.$$

Since

$$\|\hat{m}_a(\cdot; V) - m_a(\cdot; V)\|_{L_2(P_X; \mathbb{R}^J)}^2 \leq J \sup_{v \in \Pi(\mathcal{V})} \|\hat{m}_a(\cdot; v) - m_a(\cdot; v)\|_{L_2(P_X)}^2,$$

and $d_V = D_{1,V} - D_{0,V}$, we obtain

$$\sup_{V \in \mathcal{V}} P_0 \|d_V\|^2 \leq C \rho_{n_\eta}^2.$$

Thus

$$\sup_{V \in \mathcal{V}} \|\mu_V^\eta - \mu_V\| \leq \sup_{V \in \mathcal{V}} (P_0 \|d_V\|^2)^{1/2} = O_p(\rho_{n_\eta}).$$

For covariance, let $M_V^0 := P_0[z_V^0(Z)z_V^0(Z)^\top]$. Since

$$\hat{z}_V \hat{z}_V^\top - z_V^0 z_V^0{}^\top = d_V d_V^\top + d_V z_V^0{}^\top + z_V^0 d_V^\top,$$

and $\sup_{V,z} \|z_V^0(z)\| \leq B_z$,

$$\sup_{V \in \mathcal{V}} \|M_V^\eta - M_V^0\|_F = O_p(\rho_{n_\eta}).$$

Finally,

$$\Sigma_V^\eta - \Sigma_V = (M_V^\eta - M_V^0) - (\mu_V^\eta \mu_V^{\eta\top} - \mu_V \mu_V^\top),$$

and the outer-product term is $O_p(\rho_{n_\eta})$ uniformly because the means are uniformly bounded. This proves the result. □

F.4 Perturbation of the ridge criterion

Lemma F.5 (Perturbation bound). *Fix $\tau > 0$ and define*

$$Q_\tau(m, A) := m^\top (A + \tau I_J)^{-1} m$$

for $m \in \mathbb{R}^J$ and symmetric positive semidefinite $A \in \mathbb{R}^{J \times J}$. If

$$\|m\| \vee \|\tilde{m}\| \leq B,$$

then

$$|Q_\tau(m, A) - Q_\tau(\tilde{m}, \tilde{A})| \leq C(B, \tau)(\|m - \tilde{m}\| + \|A - \tilde{A}\|_F),$$

where one may take $C(B, \tau) = 2B/\tau + B^2/\tau^2$.

Proof. Let $B_A := A + \tau I_J$ and $B_{\tilde{A}} := \tilde{A} + \tau I_J$. Since $A, \tilde{A} \succeq 0$,

$$\|B_A^{-1}\|_{\text{op}} \leq \tau^{-1}, \quad \|B_{\tilde{A}}^{-1}\|_{\text{op}} \leq \tau^{-1}.$$

Decompose

$$Q_\tau(m, A) - Q_\tau(\tilde{m}, \tilde{A}) = m^\top B_A^{-1} m - \tilde{m}^\top B_A^{-1} \tilde{m} + \tilde{m}^\top (B_A^{-1} - B_{\tilde{A}}^{-1}) \tilde{m}.$$

The first term is bounded by $2B\tau^{-1}\|m - \tilde{m}\|$. For the second, use the resolvent identity

$$B_A^{-1} - B_{\tilde{A}}^{-1} = B_A^{-1}(\tilde{A} - A)B_{\tilde{A}}^{-1},$$

which gives

$$|\tilde{m}^\top (B_A^{-1} - B_{\tilde{A}}^{-1}) \tilde{m}| \leq B^2 \tau^{-2} \|A - \tilde{A}\|_F.$$

Combining the bounds proves the lemma. □

F.5 Proof of Theorem 4.1

Proof of Theorem 4.1. By Lemma F.5,

$$\sup_{V \in \mathcal{V}} |\hat{\mathcal{P}}_{\tau, \text{tr}}(V) - \mathcal{P}_\tau^\eta(V)| \leq C \left[\sup_{V \in \mathcal{V}} \|\bar{z}_{\text{tr}, V}^{\text{dr}} - \mu_V^\eta\| + \sup_{V \in \mathcal{V}} \|S_{\text{tr}, V}^{\text{dr}} - \Sigma_V^\eta\|_F \right].$$

Lemma F.3 gives

$$\sup_{V \in \mathcal{V}} |\hat{\mathcal{P}}_{\tau, \text{tr}}(V) - \mathcal{P}_\tau^\eta(V)| = O_p \left(\sqrt{\frac{Jd \log n_{\text{tr}}}{n_{\text{tr}}}} \right).$$

Similarly, Lemmas F.5 and F.4 imply

$$\sup_{V \in \mathcal{V}} |\mathcal{P}_\tau^\eta(V) - \mathcal{P}_\tau(V)| = O_p(\rho_{n_\eta}).$$

Combining these two bounds with (17) yields

$$\Delta_{\text{tr}} := \sup_{V \in \mathcal{V}} |\hat{\mathcal{P}}_{\tau, \text{tr}}(V) - \mathcal{P}_\tau(V)| = O_p \left(\sqrt{\frac{Jd \log n_{\text{tr}}}{n_{\text{tr}}}} + \rho_{n_\eta} \right).$$

It remains to prove the deterministic optimization inequality. Let

$$V_\tau^* \in \arg \max_{V \in \mathcal{V}} \mathcal{P}_\tau(V).$$

By definition of the empirical optimization gap,

$$\hat{\mathcal{P}}_{\tau, \text{tr}}(V_\tau^*) - \hat{\mathcal{P}}_{\tau, \text{tr}}(\hat{V}) \leq \varepsilon_{\text{tr}}(\hat{V}).$$

Therefore

$$\begin{aligned}\mathcal{P}_\tau(V_\tau^*) - \mathcal{P}_\tau(\hat{V}) &= \{\mathcal{P}_\tau(V_\tau^*) - \hat{\mathcal{P}}_{\tau, \text{tr}}(V_\tau^*)\} \\ &\quad + \{\hat{\mathcal{P}}_{\tau, \text{tr}}(V_\tau^*) - \hat{\mathcal{P}}_{\tau, \text{tr}}(\hat{V})\} \\ &\quad + \{\hat{\mathcal{P}}_{\tau, \text{tr}}(\hat{V}) - \mathcal{P}_\tau(\hat{V})\} \\ &\leq 2\Delta_{\text{tr}} + \varepsilon_{\text{tr}}(\hat{V}).\end{aligned}$$

If $\varepsilon_{\text{tr}}(\hat{V}) = O_p(e_{\text{tr}})$, the stochastic near-optimality statement follows immediately. \square

G Finite-dictionary location learning

For structured outcomes, Euclidean optimization may be inappropriate. A finite dictionary provides a direct alternative. Let

$$\mathcal{C} = \{c_1, \dots, c_M\} \subset \mathcal{Y}, \quad \mathcal{V}_J(\mathcal{C}) \subset \mathcal{C}^J.$$

For any output $\hat{V} \in \mathcal{V}_J(\mathcal{C})$, define its empirical dictionary optimization gap

$$\varepsilon_{\text{tr}}^{\mathcal{C}}(\hat{V}) := \sup_{V \in \mathcal{V}_J(\mathcal{C})} \hat{\mathcal{P}}_{\tau, \text{tr}}(V) - \hat{\mathcal{P}}_{\tau, \text{tr}}(\hat{V}).$$

For exhaustive search over the dictionary, this gap is zero.

Assume there exist constants $B_k, B_m, \varepsilon, \tau > 0$ such that:

- (i) for all $c \in \mathcal{C}$ and $y \in \mathcal{Y}$, $|k_Y(c, y)| \leq B_k$;
- (ii) for all $a \in \{0, 1\}$ and $x \in \mathcal{X}$, both $\pi_0(a | x)$ and $\hat{\pi}(a | x)$ are at least ε ;
- (iii) for all a, x, c , $|m_a(x; c)| \vee |\hat{m}_a(x; c)| \leq B_m$.

Define

$$\rho_{n_\eta}^{\mathcal{C}} := \sum_{a=0}^1 \left[\|\hat{\pi}(a | \cdot) - \pi_0(a | \cdot)\|_{L_2(P_X)} + \max_{c \in \mathcal{C}} \|\hat{m}_a(\cdot; c) - m_a(\cdot; c)\|_{L_2(P_X)} \right].$$

Theorem G.1 (Uniform consistency over a finite dictionary). *Fix J , suppose $n_\eta, n_{\text{tr}} \rightarrow \infty$, and assume $\rho_{n_\eta}^{\mathcal{C}} = o_p(1)$. Then*

$$\Delta_{\text{tr}}^{\mathcal{C}} := \sup_{V \in \mathcal{V}_J(\mathcal{C})} \left| \hat{\mathcal{P}}_{\tau, \text{tr}}(V) - \mathcal{P}_\tau(V) \right| = O_p \left(\sqrt{\frac{\log |\mathcal{V}_J(\mathcal{C})|}{n_{\text{tr}}}} + \rho_{n_\eta}^{\mathcal{C}} \right).$$

In particular, since $|\mathcal{V}_J(\mathcal{C})| \leq M^J$,

$$\Delta_{\text{tr}}^{\mathcal{C}} = O_p \left(\sqrt{\frac{J \log M}{n_{\text{tr}}}} + \rho_{n_\eta}^{\mathcal{C}} \right).$$

Moreover, for any output \hat{V} and any

$$V_{\tau, \mathcal{C}}^* \in \arg \max_{V \in \mathcal{V}_J(\mathcal{C})} \mathcal{P}_\tau(V),$$

$$\mathcal{P}_\tau(V_{\tau, \mathcal{C}}^*) - \mathcal{P}_\tau(\hat{V}) \leq 2\Delta_{\text{tr}}^{\mathcal{C}} + \varepsilon_{\text{tr}}^{\mathcal{C}}(\hat{V}).$$

Thus, if $\varepsilon_{\text{tr}}^{\mathcal{C}}(\hat{V}) = O_p(e_{\text{tr}}^{\mathcal{C}})$,

$$\mathcal{P}_\tau(V_{\tau, \mathcal{C}}^*) - \mathcal{P}_\tau(\hat{V}) = O_p \left(\sqrt{\frac{J \log M}{n_{\text{tr}}}} + \rho_{n_\eta}^{\mathcal{C}} + e_{\text{tr}}^{\mathcal{C}} \right).$$

Proof. Let $N_C := |\mathcal{V}_J(\mathcal{C})|$. For $i \in I_{\text{tr}}$, define

$$\hat{z}_{i,V} := z_V^{\text{dr}}(Z_i; \hat{\eta}), \quad z_{i,V}^0 := z_V^{\text{dr}}(Z_i; \eta_0).$$

Conditionally on I_η , the variables $\{\hat{z}_{i,V} : i \in I_{\text{tr}}\}$ are i.i.d. for each fixed V .

The boundedness and positivity assumptions imply

$$\|\hat{z}_{i,V}\| \vee \|z_{i,V}^0\| \leq \sqrt{J} B_z$$

for a constant $B_z < \infty$ depending only on B_k, B_m, ε . A union bound and Bernstein's inequality over the finite class give

$$\sup_{V \in \mathcal{V}_J(\mathcal{C})} \|\bar{z}_{\text{tr},V}^{\text{dr}} - \mu_V^{\hat{\eta}}\| = O_p\left(\sqrt{\frac{\log N_C}{n_{\text{tr}}}}\right),$$

and the same entrywise argument for second moments gives

$$\sup_{V \in \mathcal{V}_J(\mathcal{C})} \|\mathbf{S}_{\text{tr},V}^{\text{dr}} - \Sigma_V^{\hat{\eta}}\|_F = O_p\left(\sqrt{\frac{\log N_C}{n_{\text{tr}}}}\right).$$

The nuisance transfer bound is the same as Lemma F.4, with $\sup_{v \in \Pi(\mathcal{V})}$ replaced by $\max_{c \in \mathcal{C}}$. Hence

$$\sup_{V \in \mathcal{V}_J(\mathcal{C})} \|\mu_V^{\hat{\eta}} - \mu_V\| = O_p(\rho_{n_\eta}^{\mathcal{C}}), \quad \sup_{V \in \mathcal{V}_J(\mathcal{C})} \|\Sigma_V^{\hat{\eta}} - \Sigma_V\|_F = O_p(\rho_{n_\eta}^{\mathcal{C}}).$$

The perturbation Lemma F.5 then yields

$$\Delta_{\text{tr}}^{\mathcal{C}} = O_p\left(\sqrt{\frac{\log N_C}{n_{\text{tr}}}} + \rho_{n_\eta}^{\mathcal{C}}\right).$$

Since $N_C \leq M^J$, the displayed simplified rate follows.

Finally, by definition of the dictionary optimization gap,

$$\hat{\mathcal{P}}_{\tau, \text{tr}}(V_{\tau, \mathcal{C}}^*) - \hat{\mathcal{P}}_{\tau, \text{tr}}(\hat{V}) \leq \varepsilon_{\text{tr}}^{\mathcal{C}}(\hat{V}).$$

Adding and subtracting the empirical criterion gives

$$\mathcal{P}_\tau(V_{\tau, \mathcal{C}}^*) - \mathcal{P}_\tau(\hat{V}) \leq 2\Delta_{\text{tr}}^{\mathcal{C}} + \varepsilon_{\text{tr}}^{\mathcal{C}}(\hat{V}).$$

The stochastic bound follows immediately. □

H Implementation details

This appendix records the matrix implementation of the split-sample DR-ME test. Algorithm 1 gives the full testing pipeline. The remaining subsections define the matrices used to evaluate the training objective and the final statistic, and give the closed-form regression formulas used for the nuisance estimates.

H.1 Three-way split and matrix notation

Let

$$\{1, \dots, n\} = I_\eta \cup I_{\text{tr}} \cup I_{\text{te}}$$

be the three-way split used for nuisance fitting, location learning, and final testing. For any evaluation set $I = \{i_1, \dots, i_m\}$, let $m = |I|$, let $\mathbf{1}_m \in \mathbb{R}^m$ be the all-ones vector, and define

$$H_m := I_m - \frac{1}{m} \mathbf{1}_m \mathbf{1}_m^\top.$$

Algorithm 1 Split-sample DR-ME test with learned locations

Require: Data $Z_{1:n} = \{(X_i, A_i, Y_i)\}_{i=1}^n$, search class \mathcal{V} , number of locations J , outcome kernel k_Y , learning ridge $\tau > 0$, test ridge $\gamma_{n_{te}} > 0$, level α

Ensure: Learned locations \hat{V} , statistic $\hat{\lambda}_{n_{te}, \hat{V}}^{\text{dr}}$, p -value p_{te}^{dr}

- 1: Split the sample into disjoint sets I_η , I_{tr} , and I_{te}
- 2: Fit $\hat{\eta} = (\hat{\pi}, \hat{m}_0, \hat{m}_1)$ on I_η
- 3: **for** each candidate or optimizer evaluation $V \in \mathcal{V}$ **do**
- 4: Compute $\hat{z}_{i,V}^{\text{dr}} = z_V^{\text{dr}}(Z_i; \hat{\eta})$ for all $i \in I_{\text{tr}}$
- 5: Compute $\bar{z}_{\text{tr},V}^{\text{dr}}$ and $S_{\text{tr},V}^{\text{dr}}$
- 6: Compute

$$\hat{\mathcal{P}}_{\tau, \text{tr}}(V) = \bar{z}_{\text{tr},V}^{\text{dr}\top} (S_{\text{tr},V}^{\text{dr}} + \tau I_J)^{-1} \bar{z}_{\text{tr},V}^{\text{dr}}$$

- 7: Select $\hat{V} \in \mathcal{V}$ with small empirical gap

$$\sup_{V \in \mathcal{V}} \hat{\mathcal{P}}_{\tau, \text{tr}}(V) - \hat{\mathcal{P}}_{\tau, \text{tr}}(\hat{V}) \leq \varepsilon_{\text{tr}}$$

- 8: Compute $\hat{z}_{i,\hat{V}}^{\text{dr}} = z_{\hat{V}}^{\text{dr}}(Z_i; \hat{\eta})$ for all $i \in I_{\text{te}}$
- 9: Compute $\bar{z}_{\text{te},\hat{V}}^{\text{dr}}$ and $S_{\text{te},\hat{V}}^{\text{dr}}$
- 10: Compute

$$\hat{\lambda}_{n_{te}, \hat{V}}^{\text{dr}} = n_{te} \bar{z}_{\text{te},\hat{V}}^{\text{dr}\top} (S_{\text{te},\hat{V}}^{\text{dr}} + \gamma_{n_{te}} I_J)^{-1} \bar{z}_{\text{te},\hat{V}}^{\text{dr}}$$

- 11: Set

$$p_{te}^{\text{dr}} = 1 - F_{\chi_J^2}(\hat{\lambda}_{n_{te}, \hat{V}}^{\text{dr}})$$

- 12: Reject if $p_{te}^{\text{dr}} \leq \alpha$
-

For $V = (v_1, \dots, v_J) \in \mathcal{V}^J$, define

$$K_Y(Y_I, V) \in \mathbb{R}^{m \times J}, \quad [K_Y(Y_I, V)]_{rj} := k_Y(v_j, Y_{i_r}).$$

Thus the r -th row of $K_Y(Y_I, V)$ is $k_V(Y_{i_r})^\top$.

For $a \in \{0, 1\}$, define

$$D_{a,I} := \text{diag}\left(\frac{\mathbf{1}\{A_{i_1} = a\}}{\hat{\pi}(a | X_{i_1})}, \dots, \frac{\mathbf{1}\{A_{i_m} = a\}}{\hat{\pi}(a | X_{i_m})}\right).$$

Let $\hat{M}_{a,I}(V) \in \mathbb{R}^{m \times J}$ be the matrix of fitted arm- a regressions on I , with

$$[\hat{M}_{a,I}(V)]_{rj} = \hat{m}_a(X_{i_r}; v_j).$$

H.2 Matrix form of the pseudo-features

The arm-specific pseudo-feature matrices are

$$\hat{\Phi}_I^a(V) := D_{a,I}(K_Y(Y_I, V) - \hat{M}_{a,I}(V)) + \hat{M}_{a,I}(V), \quad a \in \{0, 1\}.$$

The doubly robust contrast matrix is

$$\hat{Z}_I(V) := \hat{\Phi}_I^1(V) - \hat{\Phi}_I^0(V) \in \mathbb{R}^{m \times J}.$$

Its r -th row is $\hat{z}_{i_r,V}^{\text{dr}\top}$. Therefore

$$\bar{z}_I^{\text{dr}}(V) = \frac{1}{m} \hat{Z}_I(V)^\top \mathbf{1}_m, \quad S_I^{\text{dr}}(V) = \frac{1}{m-1} \hat{Z}_I(V)^\top H_m \hat{Z}_I(V).$$

The empirical learning criterion on I is

$$\hat{\mathcal{P}}_{\tau,I}(V) = \bar{z}_I^{\text{dr}}(V)^\top (S_I^{\text{dr}}(V) + \tau I_J)^{-1} \bar{z}_I^{\text{dr}}(V),$$

and the final test statistic on I_{te} is

$$\hat{\lambda}_{n_{te},V}^{\text{dr}} = n_{te} \bar{z}_{I_{\text{te}}}^{\text{dr}}(V)^\top (S_{I_{\text{te}}}^{\text{dr}}(V) + \gamma_{n_{te}} I_J)^{-1} \bar{z}_{I_{\text{te}}}^{\text{dr}}(V).$$

H.3 Outcome-regression matrices

Suppose the nuisance regressions $m_a(\cdot; V)$ are estimated on I_η by kernel ridge regression with a covariate kernel k_X . The finite-feature ridge regressions used in the experiments are obtained as the corresponding linear-kernel case on the chosen feature basis.

For each arm a , let

$$I_{\eta,a} := \{i \in I_\eta : A_i = a\}, \quad n_{\eta,a} := |I_{\eta,a}|.$$

Define

$$K_{aa}^X := [k_X(X_i, X_j)]_{i,j \in I_{\eta,a}}, \quad G_{I,a}^X := [k_X(X_i, X_j)]_{i \in I, j \in I_{\eta,a}}.$$

For a location set V , define the arm- a target matrix

$$U_a(V) := K_Y(Y_{I_{\eta,a}}, V) \in \mathbb{R}^{n_{\eta,a} \times J}.$$

With ridge parameter $\lambda_a > 0$,

$$\hat{M}_{a,I}(V) = G_{I,a}^X (K_{aa}^X + \lambda_a n_{\eta,a} I_{n_{\eta,a}})^{-1} U_a(V).$$

Thus all J regression coordinates are fitted simultaneously. The matrices K_{aa}^X , $G_{I_{\text{tr}},a}^X$, and $G_{I_{\text{te}},a}^X$ do not depend on V ; only $U_a(V)$ changes with the candidate locations.

H.4 Training and testing criteria

On the training split,

$$\begin{aligned} \hat{Z}_{\text{tr}}(V) &= \hat{\Phi}_{\text{tr}}^1(V) - \hat{\Phi}_{\text{tr}}^0(V), \\ \bar{z}_{\text{tr}}^{\text{dr}}(V) &= \frac{1}{n_{\text{tr}}} \hat{Z}_{\text{tr}}(V)^\top \mathbf{1}_{n_{\text{tr}}}, \quad S_{\text{tr}}^{\text{dr}}(V) = \frac{1}{n_{\text{tr}} - 1} \hat{Z}_{\text{tr}}(V)^\top H_{n_{\text{tr}}} \hat{Z}_{\text{tr}}(V), \end{aligned}$$

and

$$\hat{\mathcal{P}}_{\tau, \text{tr}}(V) = \bar{z}_{\text{tr}}^{\text{dr}}(V)^\top (S_{\text{tr}}^{\text{dr}}(V) + \tau I_J)^{-1} \bar{z}_{\text{tr}}^{\text{dr}}(V).$$

After selecting \hat{V} , the final statistic is computed by replacing I_{tr} with I_{te} and τ with $\gamma_{n_{\text{te}}}$.

H.5 Gradient-based Euclidean optimization

When $\mathcal{Y} \subset \mathbb{R}^d$ and $k_Y(v, y)$ is differentiable in v , the criterion $V \mapsto \hat{\mathcal{P}}_{\tau, \text{tr}}(V)$ is differentiable. Let

$$R_a := (K_{aa}^X + \lambda_a n_{\eta,a} I_{n_{\eta,a}})^{-1}.$$

Since $\hat{M}_{a,I}(V) = G_{I,a}^X R_a U_a(V)$, for each location v_j ,

$$\partial_{v_j} \hat{M}_{a,I}(V) = G_{I,a}^X R_a \partial_{v_j} U_a(V).$$

The matrix $\partial_{v_j} U_a(V)$ has only one nonzero column, with entries

$$[\partial_{v_j} U_a(V)]_{rj} = \nabla_1 k_Y(v_j, Y_{i_r}), \quad i_r \in I_{\eta,a}.$$

The same structure holds for $\partial_{v_j} K_Y(Y_I, V)$.

Writing

$$\mu_I(V) := \bar{z}_I^{\text{dr}}(V), \quad A_I(V) := S_I^{\text{dr}}(V) + \tau I_J,$$

the differential of the criterion is

$$d\hat{\mathcal{P}}_{\tau,I}(V) = 2(d\mu_I(V))^\top A_I(V)^{-1} \mu_I(V) - \mu_I(V)^\top A_I(V)^{-1} (dA_I(V)) A_I(V)^{-1} \mu_I(V).$$

These formulas give analytic gradients. Automatic differentiation can also be applied directly to the matrix expressions above.

H.6 Finite-dictionary implementation

For a finite dictionary

$$\mathcal{C} = \{c_1, \dots, c_M\} \subset \mathcal{Y},$$

precompute

$$K_Y(Y_{I_{\eta,a}}, \mathcal{C}), \quad K_Y(Y_{I_{\text{tr}}}, \mathcal{C}), \quad K_Y(Y_{I_{\text{te}}}, \mathcal{C}).$$

A candidate $V = (c_{j_1}, \dots, c_{j_J}) \in \mathcal{C}^J$ is then evaluated by selecting columns j_1, \dots, j_J from these matrices. The formulas above apply without modification.

H.7 Numerical precomputation

The implementation precomputes

$$R_a, \quad G_{I_{\text{tr}},a}^X, \quad G_{I_{\text{te}},a}^X, \quad D_{a,\text{tr}}, \quad D_{a,\text{te}}, \quad a \in \{0, 1\}.$$

For each new V , the remaining operations are the construction or column selection of $K_Y(Y_I, V)$ and $U_a(V)$, followed by multiplications involving $|I| \times n_{\eta,a}$ and $n_{\eta,a} \times J$ matrices. In the finite-location regime, J is small, so the dominant cost is typically location search rather than the final Hotelling statistic.

I Additional experiments

Common synthetic setup. Unless stated otherwise, we generate $X_i \sim N(0, I_5)$ and use the confounded treatment mechanism

$$\pi_0(1 | X_i) = \text{clip}\{\sigma(0.90X_{i1} - 0.75X_{i2} + 0.55X_{i3} - 0.40X_{i4}), 0.06, 0.94\},$$

with prognostic component

$$g(x) = 0.90x_1 + 0.60 \sin(x_2) + 0.35(x_3^2 - 1) + 0.25x_1x_4 - 0.20 \cos(x_5).$$

Each sample is split into I_η , I_{tr} , and I_{te} , used respectively for nuisance fitting, location learning, and final testing. Propensities are estimated by ridge-regularized logistic regression, and the conditional kernel regressions $m_a(x; c) = E[k_Y(c, Y) | A = a, X = x]$ are estimated by multi-output ridge regression on nonlinear features of X . We use a Gaussian outcome kernel with bandwidth chosen on $I_\eta \cup I_{\text{tr}}$, a dictionary of $M = 80$ candidate outcome locations, $J = 2$ selected locations, and nominal level $\alpha = 0.05$. All rejection rates are based on 200 Monte Carlo replications; the Monte Carlo standard error at level 0.05 is approximately 0.015.

I.1 Computation infrastructure

All experiments were run locally on a professional laptop; no remote servers, cluster resources, or external GPUs were used. The reported runtimes and empirical results therefore reflect a single-machine CPU-based setup.

- **Machine:** Apple MacBook Pro
- **Model Identifier:** Mac16,1
- **Chip:** Apple M4
- **CPU:** 10 cores (4 performance cores, 6 efficiency cores)
- **Memory:** 24 GB
- **Operating System:** macOS 15.0
- **Kernel / Architecture:** Darwin 24.0.0, arm64
- **Compute:** CPU-only execution; no external GPU or remote compute was used

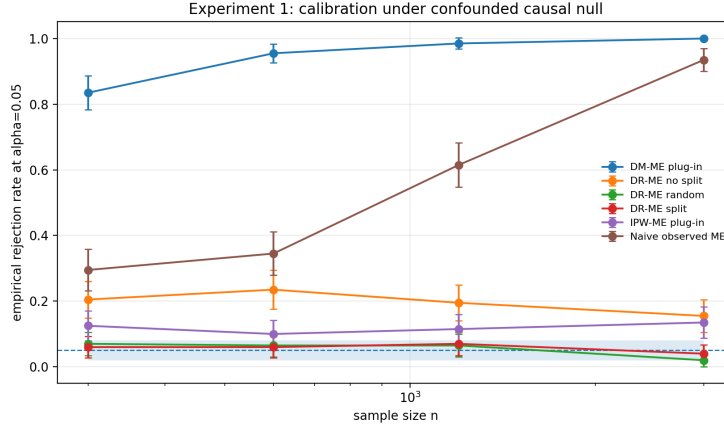


Figure 4: Sharp-null calibration under observational confounding. The dashed line is the nominal level $\alpha = 0.05$. Split DR-ME and random-location DR-ME remain calibrated; naive observed testing, no-split selection, and non-orthogonal plug-in baselines over-reject.

Table 2: Empirical rejection rates under the sharp confounded null $Y(0) = Y(1)$. The interventional laws are equal, but observed treated and control outcome distributions differ because of confounding.

Method	$n = 300$	$n = 600$	$n = 1200$	$n = 3000$
DR-ME split	0.060	0.060	0.070	0.040
DR-ME random	0.070	0.065	0.065	0.020
IPW-ME plug-in	0.125	0.100	0.115	0.135
DM-ME plug-in	0.835	0.955	0.985	1.000
Naive observed ME	0.295	0.345	0.615	0.935
DR-ME no split	0.205	0.235	0.195	0.155

I.2 Sharp-null calibration under observational confounding.

We first isolate type-I error under a sharp interventional null:

$$Y_i(0) = Y_i(1) = g(X_i) + \varepsilon_i, \quad \varepsilon_i \sim N(0, 1).$$

Thus $P_{Y(0)} = P_{Y(1)}$, but the observed treated and control outcome distributions differ because treatment depends on prognostic covariates. Figure 4 and Table 2 show that split-sample DR-ME remains close to nominal level across sample sizes, as does the random-location DR variant. By contrast, the naive observed ME test strongly over-rejects because it ignores confounding, the no-split DR-ME ablation over-rejects because locations are learned and tested on the same data, and the plug-in DM/IPW variants show the instability expected from non-orthogonal or non-augmented procedures. This experiment confirms that calibration comes from the orthogonal score together with an independent final test split.

I.3 Power under confounded alternatives.

We next use the same confounded observational design, nuisance estimators, and three-way split, but replace the sharp null by three alternatives. With $Y_i(0) = g(X_i) + \varepsilon_{i0}$, we consider a broad mean shift,

$$Y_i(1) = g(X_i) + \varepsilon_{i1} + 0.35,$$

a variance shift,

$$Y_i(1) = g(X_i) + 1.45 \varepsilon_{i1},$$

Table 3: Empirical rejection rates for DR-ME and DR-xKTE. Under the null, the entries estimate type-I error. Under the alternatives, they estimate power.

Setting	Method	$n = 300$	$n = 600$	$n = 1200$	$n = 3000$
Null	DR-ME	0.055	0.075	0.060	0.080
	DR-xKTE	0.075	0.045	0.030	0.070
Mean shift	DR-ME	0.115	0.225	0.505	0.885
	DR-xKTE	0.155	0.240	0.530	0.840
Variance shift	DR-ME	0.115	0.155	0.335	0.790
	DR-xKTE	0.065	0.080	0.190	0.560
Localized bump	DR-ME	0.135	0.165	0.225	0.605
	DR-xKTE	0.035	0.060	0.170	0.295

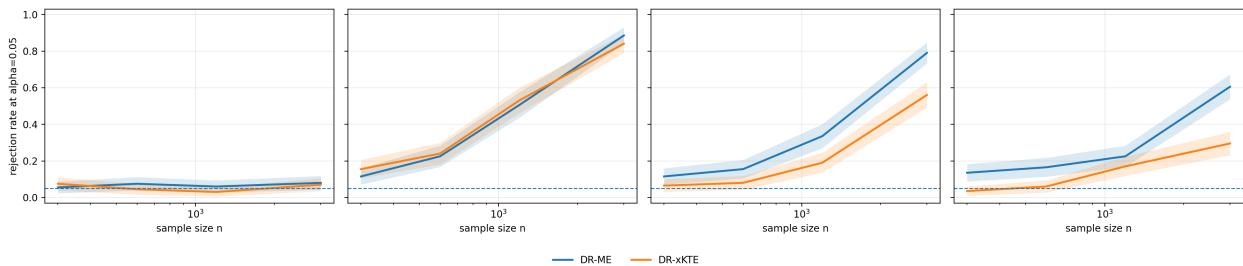


Figure 5: DR-ME versus the global DR-xKTE baseline. Both methods are close to nominal level under the confounded null. DR-ME is comparable on the mean shift and stronger on the variance-shift and localized-bump alternatives in this design.

and a mean-zero mixture perturbation,

$$Y_i(1) = g(X_i) + \varepsilon_{i1} + \frac{B_i - q}{\sqrt{q(1 - q)}}, \quad B_i \sim \text{Bernoulli}(q), \quad q = 0.12.$$

The last alternative changes the shape and tail behavior of the interventional outcome law without changing the mean of the added component. We compare DR-ME with DR-xKTE, a global doubly robust kernel test, using the same held-out test split. We also retain finite-location diagnostics from the calibration experiment: random-location DR-ME, IPW-ME, DM-ME, naive observed ME, and the no-split DR-ME ablation.

Table 3 and Figure 5 show that DR-ME and DR-xKTE have comparable calibration under the confounded null. On the broad mean-shift alternative, the two methods are similar: DR-xKTE is slightly stronger at smaller sample sizes, while DR-ME is slightly stronger at $n = 3000$. On the variance-shift and localized-bump alternatives, DR-ME is stronger at larger sample sizes. At $n = 3000$, DR-ME rejects with probabilities 0.790 and 0.605, compared with 0.560 and 0.295 for DR-xKTE. This is consistent with the finite-location objective: when a small number of whitened witness evaluations captures the discrepancy, location learning can concentrate power on informative parts of the outcome distribution rather than averaging globally.

Table 4 clarifies which rejection rates can be interpreted as calibrated power. The naive observed ME test rejects the null with probability 0.960, because it tests observed treated-versus-control outcome distributions rather than interventional laws. The no-split ablation also over-rejects, showing the selection bias induced by learning and testing locations on the same data. The DM plug-in baseline is not a valid calibrated comparator in this experiment, since it has near-unit null rejection. The calibrated comparison is therefore mainly among DR-ME, DR-ME-Rand, and DR-xKTE. Within that group, learned locations improve over random locations, and DR-ME gives the largest rejection rates on the variance and localized-bump alternatives.

Table 4: Diagnostic baselines at $n = 3000$. These baselines are included to interpret the power curves, not all as valid calibrated competitors.

Method	Null	Mean shift	Variance shift	Localized bump
DR-ME	0.080	0.885	0.790	0.605
DR-xKTE	0.070	0.840	0.560	0.295
DR-ME-Rand	0.045	0.830	0.690	0.475
IPW-ME plug-in	0.110	0.685	0.590	0.590
DM-ME plug-in	0.990	1.000	1.000	1.000
Naive observed ME	0.960	1.000	0.990	0.980
DR-ME-NoSplit	0.190	0.965	0.880	0.845

I.4 High-dimensional location-learning ablation

This experiment isolates the role of the covariance-whitened learning criterion. The final test is held fixed across methods: all variants compute the same split-sample DR-ME Hotelling statistic on I_{te} . Only the location-learning rule on I_{tr} changes. We compare full whitening,

$$\hat{\mu}_V^\top (\hat{\Sigma}_V + \tau I)^{-1} \hat{\mu}_V,$$

raw witness maximization, $\|\hat{\mu}_V\|^2$, and random dictionary locations.

Outcomes are vector-valued, $Y \in \mathbb{R}^{d_Y}$, with $d_Y \in \{5, 10, 25, 50\}$. Under the null,

$$Y(0) = Y(1) = \mu(X) + \varepsilon.$$

Under the alternative, rare mass is shifted toward two sparse regions:

$$Y(0) = \mu(X) + \varepsilon_0 - \Delta v_1 \mathbf{1}\{B_0 = 1\} - \Delta v_2 \mathbf{1}\{B_0 = 2\},$$

$$Y(1) = \mu(X) + \varepsilon_1 + \Delta v_1 \mathbf{1}\{B_1 = 1\} + \Delta v_2 \mathbf{1}\{B_1 = 2\},$$

where $\Pr(B_a = 1) = \Pr(B_a = 2) = 0.04$ and $\Delta = 4$. Candidate locations are observed outcomes from the training split, so most dictionary points are background points rather than bump locations. We use $n = 3000$, $M = 300$ dictionary candidates, $J = 3$ selected locations, and 200 Monte Carlo replications.

The main text reports null rejection rates and power. Here we report selection diagnostics explaining the power gap.

Table 5 shows that full whitening selects informative and less redundant coordinates. It hits at least one true bump region much more often than random locations, and it selects more distinct bump regions than the raw witness objective. It also has lower average feature correlation than raw witness maximization. Thus the gain in the main power table is not merely from finding large empirical witness values: the covariance term changes the selected finite-dimensional projection by penalizing redundant or high-noise coordinates, as predicted by the criterion $\mu_V^\top \Sigma_V^{-1} \mu_V$.

I.5 Local noncentral chi-square validation

This experiment validates the local asymptotic law of the fixed-location orthogonalized ME statistic. Unlike the previous power experiments, the goal is not to compare against external baselines. The goal is to check whether, once the locations are fixed independently of the test sample, the empirical Hotelling statistic follows the predicted central and noncentral chi-square laws.

The theoretical prediction is the following. For fixed locations V and local alternatives of size $n^{-1/2}$,

$$\sqrt{n} \bar{z}_{n,V}^{\text{dr}} \Rightarrow N(h\eta_V(g), \Sigma_V), \tag{18}$$

Table 5: Selection diagnostics under the high-dimensional two-bump alternative. "Any bump" is the probability that at least one selected location lies in a true bump region. "Distinct regions" is the average number of distinct bump regions selected. "Avg. corr." is the average absolute correlation among the selected DR features on the training split.

d_Y	Method	Any bump	Distinct regions	Avg. corr.
5	DR-ME	1.000	2.495	0.173
	Raw witness	0.180	0.205	0.765
	Random locations	0.200	0.230	0.384
10	DR-ME	1.000	2.240	0.170
	Raw witness	0.295	0.315	0.646
	Random locations	0.245	0.270	0.383
25	DR-ME	0.870	1.470	0.248
	Raw witness	0.420	0.500	0.529
	Random locations	0.205	0.210	0.378
50	DR-ME	0.890	1.300	0.274
	Raw witness	0.750	1.010	0.434
	Random locations	0.210	0.220	0.360

and therefore

$$\widehat{\lambda}_{n,V}^{\text{dr}} = n \bar{z}_{n,V}^{\text{dr}\top} (S_{n,V}^{\text{dr}} + \gamma_n I_J)^{-1} \bar{z}_{n,V}^{\text{dr}} \Rightarrow \chi_J^2(h^2 \lambda_V(g)), \quad (19)$$

where

$$\lambda_V(g) = \eta_V(g)^\top \Sigma_V^{-1} \eta_V(g). \quad (20)$$

Thus, under the null $h = 0$, the statistic should be approximately central χ_J^2 . Under local alternatives, the rejection probability should follow the power curve of a noncentral χ_J^2 distribution with noncentrality parameter $h^2 \lambda_V(g)$.

We use the same observational structure as in the previous experiments:

$$X_i \sim N(0, I_5), \quad A_i | X_i \sim \text{Bernoulli}(\pi_0(X_i)), \quad (21)$$

with

$$\pi_0(1 | X_i) = \text{clip}\{\sigma(0.90X_{i1} - 0.75X_{i2} + 0.55X_{i3} - 0.40X_{i4}), 0.06, 0.94\}. \quad (22)$$

The prognostic component is

$$g(x) = 0.90x_1 + 0.60 \sin(x_2) + 0.35(x_3^2 - 1) + 0.25x_1x_4 - 0.20 \cos(x_5). \quad (23)$$

The local path is a treatment-arm mean shift of order $n^{-1/2}$:

$$Y_i(0) = g(X_i) + \varepsilon_{i0}, \quad Y_i(1) = g(X_i) + \varepsilon_{i1} + \delta_n, \quad \delta_n = \frac{h}{\sqrt{n}}, \quad (24)$$

with $\varepsilon_{i0}, \varepsilon_{i1} \sim N(0, 1)$. The treatment mechanism and the covariate distribution are unchanged along the path. Hence the only local perturbation is in the interventional outcome law under treatment.

We use a Gaussian kernel on the outcome. Since the conditional residual law is Gaussian, the nuisance regressions

$$m_a(x; v) = E[k_Y(v, Y) | A = a, X = x]$$

are available in closed form. For $Y = g(x) + \delta + \varepsilon$, $\varepsilon \sim N(0, \sigma_Y^2)$, and $k_Y(v, y) = \exp\{-(v - y)^2 / (2\ell_Y^2)\}$,

$$m_\delta(x; v) = \left(\frac{\ell_Y^2}{\ell_Y^2 + \sigma_Y^2} \right)^{1/2} \exp\left\{ -\frac{(v - g(x) - \delta)^2}{2(\ell_Y^2 + \sigma_Y^2)} \right\}. \quad (25)$$

Table 6: Empirical rejection rates under local alternatives, compared with the noncentral chi-square prediction. The theoretical power is computed from $\chi_2^2(h^2\hat{\lambda}_V)$ with $\hat{\lambda}_V = 0.1383$.

h	$h^2\hat{\lambda}_V$	Theory	$n = 500$	$n = 1000$	$n = 3000$
0	0.000	0.050	0.053	0.044	0.054
1	0.138	0.061	0.063	0.059	0.049
2	0.553	0.094	0.107	0.101	0.095
3	1.245	0.155	0.164	0.166	0.167
4	2.213	0.246	0.260	0.269	0.275
6	4.979	0.502	0.555	0.519	0.524
8	8.851	0.763	0.810	0.786	0.770

We use these true nuisance functions in this experiment to isolate the local chi-square approximation from nuisance-estimation error. This is a deliberate theory-validation experiment: first-stage estimation is not the object being tested here.

The locations are also fixed independently of the Monte Carlo testing samples. A large independent pilot sample under the null is used to select $J = 2$ locations by maximizing the local noncentrality proxy

$$\eta_V^\top (\Sigma_V + \tau I_J)^{-1} \eta_V. \quad (26)$$

The selected locations are then frozen for all repetitions, all sample sizes, and all local-alternative strengths. This avoids any leakage from the test sample into the location choice.

The pilot configuration is:

$$n_{\text{pilot}} = 100000, \quad (27)$$

$$M = 100, \quad (28)$$

$$J = 2, \quad (29)$$

$$\hat{V} = (-2.6752, 3.9031), \quad (30)$$

$$\ell_Y = 1.4289, \quad (31)$$

$$\hat{\lambda}_V = 0.1383. \quad (32)$$

We then run 2000 Monte Carlo repetitions for each $n \in \{500, 1000, 3000\}$ and $h \in \{0, 1, 2, 3, 4, 6, 8\}$. The rejection threshold is the 0.95 quantile of χ_2^2 .

Table 6 shows that the empirical rejection probabilities closely follow the noncentral chi-square prediction. Under the null, corresponding to $h = 0$, the rejection rate is approximately 5% at all sample sizes. This verifies the central chi-square calibration of the fixed-location statistic. Under local alternatives, the rejection probability increases with h and tracks the theoretical curve well. The agreement is especially good at $n = 1000$ and $n = 3000$, as expected from an asymptotic local theory.

At the smaller sample size $n = 500$, the empirical power is slightly above the asymptotic prediction for larger values of h , especially at $h = 6$ and $h = 8$. This is not a failure of the theory. For large h , the finite-sample shift $\delta_n = h/\sqrt{n}$ is no longer extremely small, so the experiment is moving away from the strictly local regime. The asymptotic prediction should be most accurate when n is larger and the same h corresponds to a smaller actual shift.

Figure 6 is the main figure for the experiment. It directly validates the local-power formula. The horizontal axis is the local strength h , not the raw shift δ_n . The raw shift changes with n as $\delta_n = h/\sqrt{n}$, while the theory predicts that the asymptotic power should depend on h through $h^2\lambda_V$. The empirical curves are close to the theoretical curve, which supports the claim that λ_V is the relevant whitened local signal-to-noise ratio.

Figure 7 checks the full null distribution, not only the rejection probability at level 0.05. The empirical histogram aligns well with the central χ_2^2 reference law. This supports the fixed-location null calibration of the statistic and confirms that the covariance normalization is working as intended.

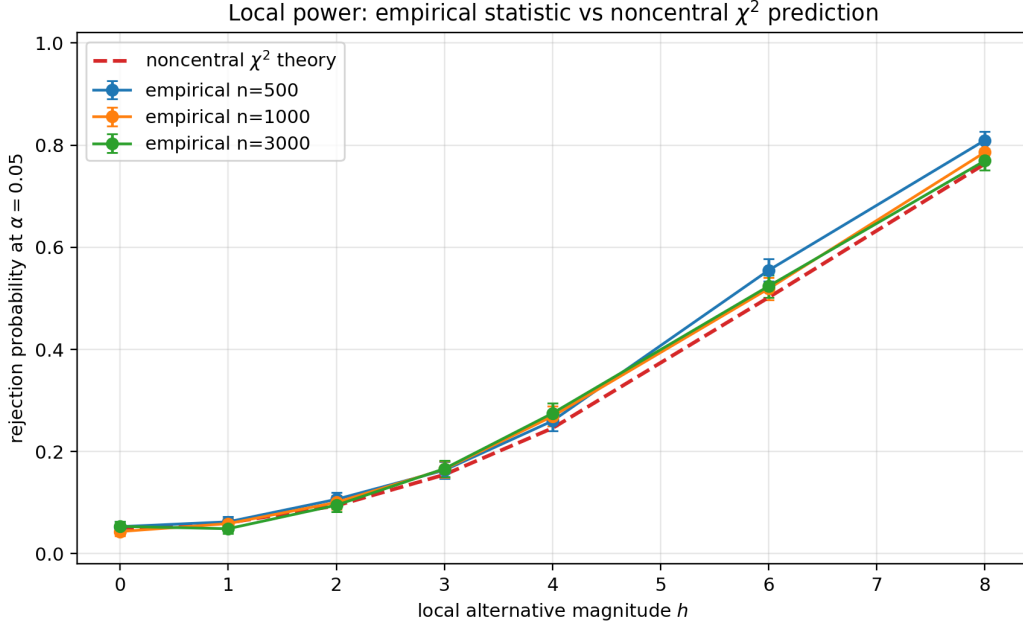


Figure 6: Empirical rejection rates against the noncentral chi-square prediction. The black theoretical curve is computed from $\chi^2_2(h^2\hat{\lambda}_V)$. The empirical curves for $n = 500, 1000, 3000$ closely follow the predicted local-power curve, with the largest-sample curve giving the closest agreement.

Figure 8 gives a stronger distributional diagnostic. A power curve only checks one tail probability for each h , whereas the QQ plot checks the entire distribution. The approximate alignment with the diagonal indicates that the statistic is not merely producing the correct rejection probability, but is close to the predicted noncentral chi-square distribution over a broad range of quantiles.

Figure 9 compares the empirical first moment of the statistic with the theoretical mean of the limiting noncentral chi-square law:

$$E[\chi^2_J(h^2\lambda_V)] = J + h^2\lambda_V. \quad (33)$$

The empirical means follow this prediction closely. The mild upward deviation for larger h at smaller n is consistent with the finite-sample behavior already visible in the power curves: for large local strengths and moderate n , the alternatives are no longer perfectly infinitesimal.

Overall, this experiment supports the local asymptotic theory in two ways. First, under $h = 0$, the statistic has the predicted central chi-square behavior. Second, under $n^{-1/2}$ local alternatives, its rejection probability and distributional shape are well described by the noncentral chi-square law with noncentrality parameter $h^2\lambda_V$. This validates the main theoretical interpretation of the statistic and justifies using the whitened quantity λ_V as the target criterion for location learning.

Once V is fixed independently of the test sample, the statistic behaves exactly as the local Gaussian and noncentral chi-square theory predicts.

I.6 Runtime comparison with a global DR kernel test

We finally compare the computational cost of the proposed finite-location test against a global doubly robust kernel treatment-effect test. The purpose of this experiment is not to study power, but to quantify the practical cost of the two ways of implementing DR-ME and to compare them with DR-xKTE. The comparison is important because DR-ME ultimately tests a low-dimensional statistic indexed by J learned locations, whereas DR-xKTE remains a global kernel statistic over the evaluation sample.

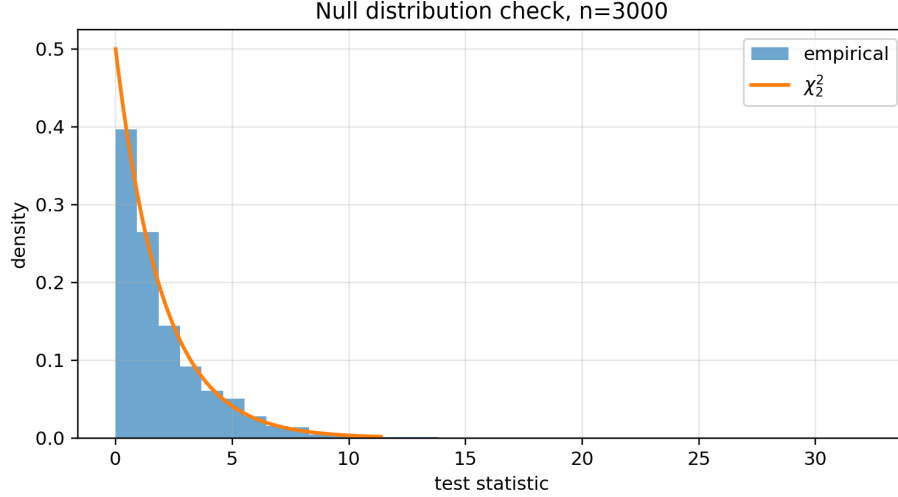


Figure 7: Null distribution of the statistic at the largest sample size. The histogram shows the Monte Carlo distribution of $\hat{\lambda}_{n,V}^{\text{dr}}$ under $h = 0$, while the curve shows the central χ_2^2 density.

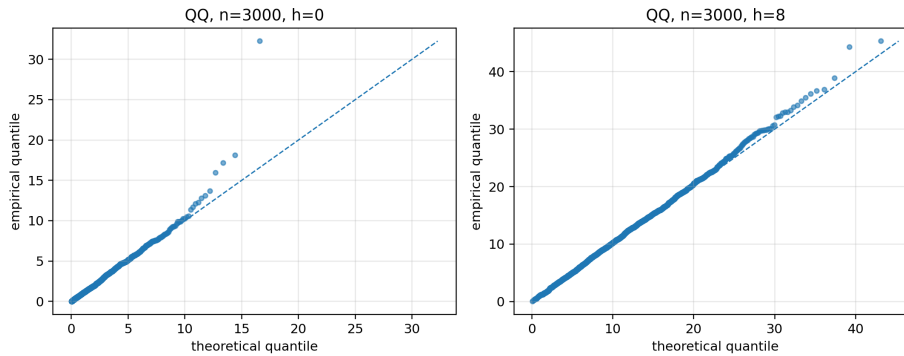


Figure 8: QQ plot at the largest sample size. Empirical quantiles of the statistic are compared with the corresponding noncentral chi-square quantiles.

We use the same observational data-generating mechanism as in the previous experiments and the same three-way split

$$\{1, \dots, n\} = I_\eta \cup I_{\text{tr}} \cup I_{\text{te}}.$$

The nuisance split I_η is used to fit the propensity and, for DR-ME, the conditional kernel regressions. The training split I_{tr} is used to learn locations for DR-ME, and the final test is evaluated on I_{te} . This split is kept fixed across implementations so that the measured difference is due to the testing procedure rather than to different data usage.

We compare three methods:

- **DR-ME-Dict:** the finite-dictionary implementation of DR-ME. A dictionary $C = \{c_1, \dots, c_M\}$ of candidate outcome locations is formed, all outcome-kernel evaluations $K_Y(Y, C)$ are precomputed, and locations are selected by greedy maximization of the ridge-stabilized local-power criterion. We use $J = 2$ selected locations and $M = 80$ dictionary candidates.
- **DR-ME-Grad:** the continuous-location implementation of DR-ME. Locations are optimized by gradient

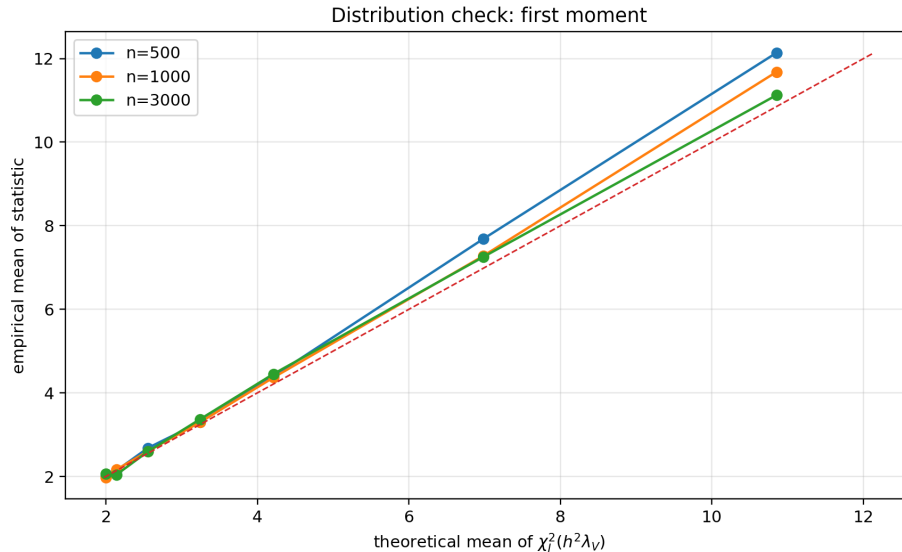


Figure 9: Moment diagnostic. The empirical mean of $\hat{\lambda}_{n,V}^{\text{dr}}$ is compared with the theoretical mean $J + h^2\hat{\lambda}_V$ of the noncentral χ_J^2 distribution.

Table 7: Total runtime in seconds. Total runtime includes nuisance fitting, location learning when applicable, and final testing. Results are averaged over five random seeds with $J = 2$, $M = 80$, and three gradient steps for DR-ME-Grad.

n	DR-ME-Dict	DR-ME-Grad	DR-xKTE
300	0.0048	0.0019	0.0006
600	0.0059	0.0032	0.0012
1200	0.0132	0.0107	0.0046
3000	0.0223	0.0282	0.0366
5000	0.0395	0.0508	0.1252
10000	0.2080	0.3631	0.9982

ascent in the Euclidean outcome space, using the differentiable version of the same ridge-stabilized criterion. We use three gradient steps in this runtime experiment.

- **DR-xKTE**: a global doubly robust kernel test for the kernel treatment effect. The propensity is fit on I_η and evaluated on I_{te} , as in DR-ME. The statistic is then computed on the final test split. We use a Cholesky-based linear solver for the internal kernel ridge systems, so this is not an intentionally slow implementation.

For each method, we decompose runtime into nuisance fitting, location learning when applicable, and final testing. For DR-ME-Dict, the learning time includes precomputing the dictionary kernel matrices and greedy location search. For DR-ME-Grad, the learning time is the continuous gradient-ascent optimization. For DR-xKTE, there is no location-learning phase; the method-specific cost is the global kernel statistic computed on I_{te} . We report averages over five random seeds for each sample size

$$n \in \{300, 600, 1200, 3000, 5000, 10000\}.$$

Table 7 and Figure 10 show that the relative cost changes with sample size. For $n \leq 1200$, all methods are cheap, and DR-xKTE is often the fastest method. This is expected: at small sample sizes, the

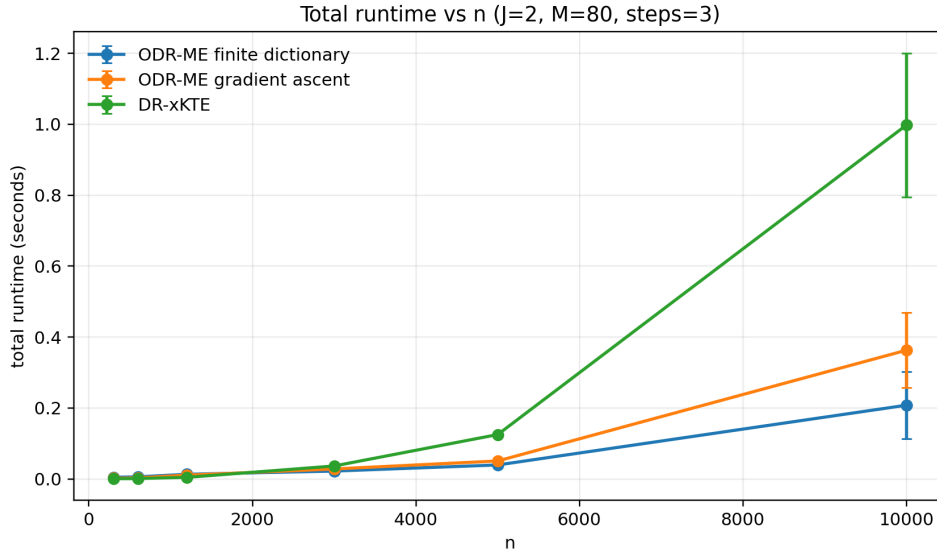


Figure 10: Total runtime versus sample size. DR-xKTE is competitive at small sample sizes, where the global kernel computation is still cheap. At larger sample sizes, the finite-dictionary DR-ME implementation becomes faster. Continuous gradient ascent becomes the most expensive implementation at large n , even with only three gradient steps.

overhead of precomputing dictionary features and running location search is not yet offset by DR-ME’s low-dimensional final statistic. At $n = 3000$, DR-xKTE remains slightly faster than DR-ME-Dict in this optimized implementation. However, for $n = 5000$ and $n = 10000$, DR-ME-Dict becomes faster than DR-xKTE. At $n = 10000$, DR-ME-Dict is faster than DR-xKTE.

This scaling is the relevant practical point. DR-xKTE is a global kernel test and therefore continues to manipulate kernel matrices on the evaluation sample. In contrast, after location learning, DR-ME computes a Hotelling statistic in only $J = 2$ dimensions. The finite-dictionary implementation also exploits the fact that all candidate outcome-kernel evaluations can be precomputed once and reused during greedy search.

The core-runtime comparison in Table 8 and Figure 11 gives the cleanest view of method-specific scaling. Nuisance fitting is shared in spirit across the methods and is not the main object of the comparison. The core runtime shows that DR-ME-Dict is not uniformly faster than DR-xKTE at every sample size, but it becomes faster in the large- n regime. This is the regime where using a small number of learned locations matters computationally.

The continuous gradient implementation has a different profile. It avoids a finite dictionary and therefore its cost does not depend on M , but each gradient step requires evaluating the full criterion and its derivative over the training split. With three gradient steps, it is already slower than DR-ME-Dict at $n \geq 3000$. Increasing the number of gradient steps would further increase this gap. Therefore, continuous gradient ascent is useful as an alternative for low-dimensional Euclidean outcomes, but it should not be the default scalable implementation in the current empirical suite.

Figure 12 shows the breakdown at the largest sample size. The finite-dictionary implementation is the most attractive option: it is faster than DR-xKTE at $n = 10000$ and still returns learned interpretable locations. DR-xKTE remains a strong global baseline, but its runtime is tied to a global kernel computation over the evaluation sample. DR-ME-Grad is dominated by its repeated gradient evaluations and is therefore less attractive for large n .

Overall, this experiment supports a task-dependent implementation choice. For hypothesis testing, as in our main experiments, DR-ME is best implemented with a finite dictionary and small J . This yields a

Table 8: Core method runtime in seconds. Core runtime removes nuisance fitting and keeps only location learning plus the final test for DR-ME, or the global kernel statistic for DR-xKTE. Results are averaged over five random seeds with $J = 2$, $M = 80$, and three gradient steps for DR-ME-Grad.

n	DR-ME-Dict	DR-ME-Grad	DR-xKTE
300	0.0037	0.0007	0.0004
600	0.0038	0.0011	0.0010
1200	0.0054	0.0030	0.0043
3000	0.0140	0.0200	0.0359
5000	0.0296	0.0409	0.1236
10000	0.1924	0.3475	0.9964

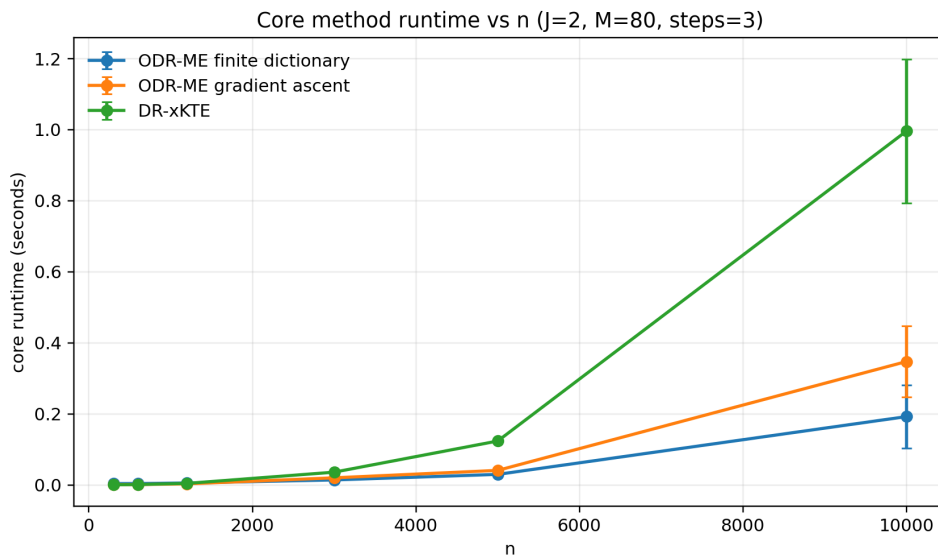


Figure 11: Core method runtime versus sample size. This plot removes nuisance fitting and focuses on the computational cost specific to the test. The finite-dictionary implementation of DR-ME overtakes DR-xKTE at large n , while the gradient implementation becomes substantially slower.

practical low-dimensional test, scales favorably at larger sample sizes, and preserves interpretability through selected outcome locations. Continuous gradient learning is better viewed as an optional Euclidean-location variant: it is natural when the goal is to optimize interpretable locations in structured Euclidean outcome spaces, such as images, but it is not the primary scalable implementation for testing. DR-xKTE remains the main global-kernel baseline for power comparisons, while the runtime results show that finite-location testing can provide a computational advantage in the larger- n regime.

I.7 OCTMNIST mean-matched image-location experiment

We use OCTMNIST from MedMNIST v2 [39], [18]. MedMNIST v2 is released under the Creative Commons Attribution 4.0 International license (CC BY 4.0). OCTMNIST is used to construct a semi-synthetic observational experiment with full image outcomes. The main goal is to study whether a learned finite-location witness can localize a causal distributional change in image space, while avoiding the degenerate setup in which the same image serves both as a covariate and as an outcome. We therefore generate low-dimensional pre-treatment covariates synthetically, use them to induce confounding and heterogeneity,

Table 9: Runtime breakdown in seconds at $n = 10000$, with $J = 2$, $M = 80$, and three gradient steps for DR-ME-Grad. Entries are averages over five random seeds.

Method	Nuisance	Learning	Test	Total
DR-ME-Dict	0.0156	0.1236	0.0688	0.2080
DR-ME-Grad	0.0156	0.3033	0.0441	0.3631
DR-xKTE	0.0017	0.0000	0.9964	0.9982

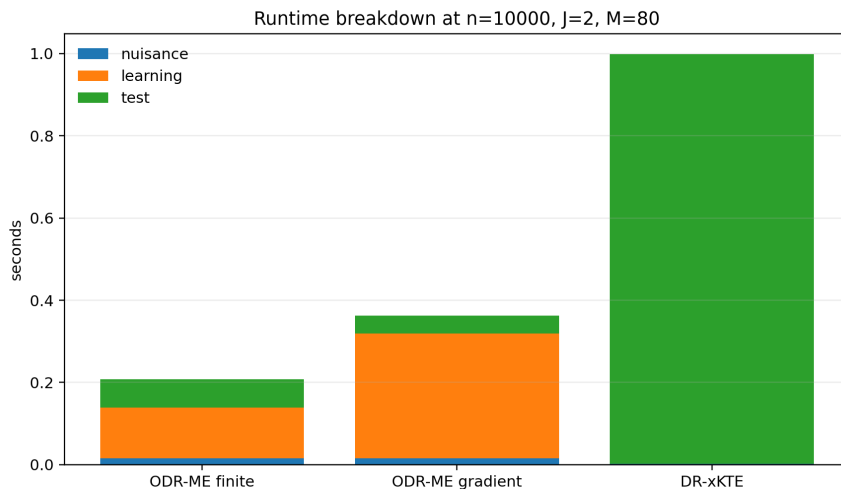


Figure 12: Runtime breakdown at $n = 10000$, $J = 2$, and $M = 80$. The finite-dictionary DR-ME implementation keeps the final test low-dimensional and is faster than DR-xKTE, whose cost is dominated by the global kernel test. Gradient-based DR-ME spends most of its time in location learning.

and use OCTMNIST images only on the outcome side.

For each unit, we first sample synthetic covariates

$$X_i \in \mathbb{R}^{d_X}, \quad X_i \sim N(0, I_{d_X}),$$

with $d_X = 6$ in our implementation. Treatment is assigned observationally by a clipped logistic propensity,

$$A_i | X_i \sim \text{Bernoulli}\{\pi_0(1 | X_i)\}, \quad \pi_0(1 | X_i) = \text{clip}\{\sigma(\alpha^\top X_i), 0.07, 0.93\},$$

so confounding is driven by the synthetic covariates rather than by the OCT images themselves.

The outcome construction begins with baseline images

$$B_i \in [0, 1]^{28 \times 28}$$

sampled from the *normal* OCTMNIST class. These images play the role of untreated anatomy. To define a clinically interpretable treatment pattern, we construct a fixed fluid-like template

$$M \in [0, 1]^{28 \times 28}$$

from OCTMNIST using the positive part of the smoothed mean difference between the DME and normal classes, together with a mild central spatial prior. The DME images are therefore used only to define this template; the causal sample itself is built from normal baseline images.

Table 10: Total runtime in seconds as the number of locations J varies, with $n = 1200$, $M = 80$, and three gradient steps for DR-ME-Grad. Results are averaged over five random seeds.

J	DR-ME-Dict	DR-ME-Grad	DR-xKTE
1	0.0133	0.0118	0.0043
2	0.0158	0.0128	0.0058
5	0.0187	0.0108	0.0044
10	0.0320	0.0128	0.0046

Table 11: Total runtime in seconds as the dictionary size M varies, with $n = 1200$, $J = 2$, and three gradient steps for DR-ME-Grad. Results are averaged over five random seeds.

M	DR-ME-Dict	DR-ME-Grad	DR-xKTE
40	0.0114	0.0109	0.0052
80	0.0139	0.0113	0.0039
160	0.0184	0.0111	0.0043
320	0.0260	0.0106	0.0045

Potential outcomes are generated by adding treatment-specific residual images to the same baseline anatomy:

$$Y_i(a) = B_i + R_i(a), \quad a \in \{0, 1\}.$$

The residuals are designed so that the two treatment arms have the same average residual signal, but different residual distributions. Let

$$q_i = q_{\min} + (q_{\max} - q_{\min}) \sigma(\beta^\top X_i),$$

where $q_i \in (q_{\min}, q_{\max})$ is a covariate-dependent probability of a severe fluid event. We then sample

$$S_i \mid X_i \sim \text{Bernoulli}(q_i),$$

and define mean-one multiplicative amplitude jitters

$$J_{ia} = \exp(\tau U_{ia} - \tau^2/2), \quad U_{ia} \sim N(0, 1).$$

The two residual laws are

$$R_i(0) = q_i \theta J_{i0} M + \varepsilon_{i0}, \quad R_i(1) = S_i \theta J_{i1} M + \varepsilon_{i1},$$

with independent Gaussian pixel noise

$$\varepsilon_{i0}, \varepsilon_{i1} \sim N(0, \sigma^2 I).$$

Since $\mathbb{E}[J_{ia}] = 1$ and $\mathbb{E}[S_i \mid X_i] = q_i$, the construction satisfies

$$\mathbb{E}\{R_i(1) - R_i(0) \mid X_i\} = 0.$$

Thus the treatment effect is distributional rather than mean-based: the control arm carries a mild diffuse fluid pattern, while the treated arm exhibits rare but much more severe localized deviations.

In finite samples, the equality above holds exactly only in expectation. To make the oracle mean residual difference visually and numerically null in the realized sample, we additionally recenter the sampled residuals. Writing

$$\bar{\Delta}_R := \frac{1}{n} \sum_{i=1}^n \{R_i(1) - R_i(0)\},$$

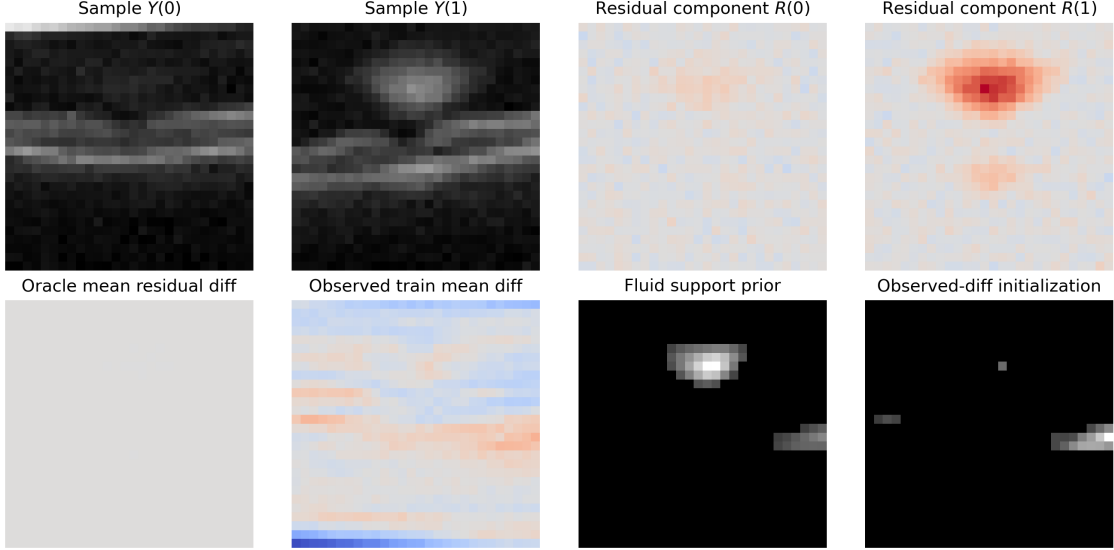


Figure 13: Additional diagnostics for the OCTMNIST mean-matched image-location experiment. Top row: sampled control and treated images $Y(0)$, $Y(1)$, together with their residual components $R(0)$, $R(1)$. Bottom row: oracle mean residual difference, observed treated-versus-control mean image difference on the training split, the fluid support prior, and the observed-difference initialization. The learned DR-ME image location shown in the main text is optimized from this initialization on the training split and evaluated only on the independent test split. After sample-level recentering, the oracle mean residual difference is zero up to numerical precision, so localization is not driven by a residual mean shift.

we replace

$$R_i(0) \leftarrow R_i(0) + \frac{1}{2}\bar{\Delta}_R, \quad R_i(1) \leftarrow R_i(1) - \frac{1}{2}\bar{\Delta}_R.$$

After this recentering, the empirical oracle residual mean difference is zero up to numerical precision, while the residual distributions remain different. This makes the qualitative localization diagnostic sharper: any visually meaningful learned location cannot be attributed to a first-moment residual contrast.

The observed outcome is

$$Y_i = A_i Y_i(1) + (1 - A_i) Y_i(0).$$

For inference we work directly with the full image outcomes, not with residuals. We use a Gaussian image kernel

$$k_Y(v, y) = \exp\left\{-\frac{\|v - y\|_2^2}{2d_Y \ell_Y^2}\right\}, \quad d_Y = 28 \cdot 28,$$

where the factor d_Y makes ℓ_Y interpretable as a per-pixel scale. The propensity is estimated on I_η by logistic regression, and the nuisance regressions

$$m_a(x; v) = \mathbb{E}\{k_Y(v, Y) \mid A = a, X = x\}$$

are estimated on I_η by ridge regression over a fixed nonlinear feature basis of X .

We learn a single image location v on the training split I_{tr} , so $J = 1$. In this scalar case, the DR-ME location-learning criterion reduces to the squared standardized doubly robust moment,

$$v \mapsto \hat{\mathcal{P}}_{\tau, \text{tr}}(v) = \frac{\bar{z}_{\text{tr}}^{\text{dr}}(v)^2}{\widehat{\text{Var}}_{\text{tr}}\{z^{\text{dr}}(v)\} + \tau}.$$

The final one-location DR-ME statistic is then computed only on the independent test split I_{te} .

Because v lives in a continuous 28×28 image space, direct first-order optimization is highly nonconvex and, without further structure, often returns diffuse or anatomically implausible solutions. We therefore use a small amount of optimization-side regularization to stabilize the search and to favor interpretable image locations. First, the optimization is initialized at the observed treated-versus-control mean image difference on the training split,

$$v_{\text{init}} = \bar{Y}_{\text{tr},A=1} - \bar{Y}_{\text{tr},A=0}.$$

Second, each gradient step is smoothed by a Gaussian filter and lightly anchored toward the initialization, which discourages unstable high-frequency updates. These operations are used only to stabilize the continuous optimization problem and to improve interpretability; they do not use the test split and do not alter the final split-sample DR-ME statistic once the location has been learned. In the plotted figures, an additional display threshold is applied only for visualization, so that faint background structure is suppressed and the dominant localized region is easier to see.

This experiment should therefore be interpreted as a qualitative localization diagnostic rather than as a benchmark for unconstrained image optimization. It shows that, once the average residual contrast is removed, a learned finite location can still localize the retinal region where the interventional image laws differ. At the same time, the need for smoothness, support, and sparsity aids highlights an interesting methodological direction: for structured outcomes such as images, more principled optimization classes for v may be preferable to unconstrained pixel-space search. Possible future directions include sparse or wavelet-based parameterizations, total-variation or shape-constrained regularization, learned dictionaries of candidate image locations, and other structured search classes that preserve the split-sample DR-ME testing logic while making location learning more stable and more interpretable.